Comparing a diquark-antidiquark and a mesonic molecule creation operator for a $\bar{b}\bar{b}ud$ tetraquark

MASTER THESIS

Sebastian Velten

September 24, 2020

Institut für theorethische Physik
J.W. Goethe Universität Frankfurt a.M.

Supervisor and 1st examiner: Prof. Marc Wagner
2nd examiner: Prof. Owe Philipsen

Zusammenfassung

In dieser Arbeit werden zwei Strukturen (Diquark-Antidiquark und mesonisches Molekül) mit Hilfe von Gitter-QCD Methoden für ein $\bar{b}\bar{b}ud$ Tetraquark verglichen, für das bereits ein gebundener Zustand mit den Quantenzahlen $I(J^P) = 0(1^+)$ postuliert wurde. Das Tetraquark wird dabei in der statisch-leichten Näherung betrachtet. Das bedeutet, dass das $\bar{b}\bar{b}$ Paar als unendlich schwer (statisch) betrachtet wird, während die leichten u/d Quarks voll dynamisch sind. Die beiden Strukturen zu vergleichen bedeutet konkret, zu untersuchen welche Struktur (im Vergleich zur anderen) die bessere Beschreibung für den Grundzustand des Tetraquarks liefert. Der erste Schritt zur Beantwortung dieser Fragestellung ist das Berechnen einer 2×2 Korrelationsmatrix aus den beiden Zuständen. Anschließend wird das verallgemeinerte Eigenwertproblem (GEVP) gelöst und die relative Gewichtung der beiden Zustände aus dem resultierenden (Grundzustands-) Eigenvektor extrahiert. Es stellt sich heraus, dass der Diquark-Antidiquark Zustand für sehr kleine Abstände der schweren Quarks dominiert und für größer werdende Abstände immer mehr an Bedeutung verliert, sodass hier schließlich nur noch das mesonische Molekül beiträgt. Als Zwischenresultat wird ebenfalls das Potential der statischen Antiquarks in Anwesenheit der leichten Quarks berechnet und analysiert.

Abstract

In this master thesis, lattice QCD methods are used to compare two structures (diquark-antidiquark and mesonic molecule) for a $\bar{b}\bar{b}ud$ tetraquark, for which a bound state with quantum numbers $I(J^P) = 0(1^+)$ has already been predicted. The tetraquark is treated in the static-light approximation. That means, that the $\bar{b}\bar{b}$ pair is assumed to be infinitely heavy (static), while the light u/d quarks are treated fully relativistically. To be more precise, comparing both structures means to investigate which structure is the better description for the tetraquark ground state (compared to the other structure). The first step in answering this question is the computation of a 2×2 correlation matrix from the both states. Afterwards one has to solve the generalized eigenvalue problem (GEVP) and then the relative weight for both states can be extracted from the resulting (ground state-) eigenvector. It turns out, that the diquark-antidiquark state dominates for very small heavy quark separations, but it becomes more and more negligible for larger separations, where the tetraquark can be seen as pure mesonic molecule state. As an intermediate result also the potential of the static antiquarks in the presence of the light quarks is computed and analyzed.

Contents

1 Introduction

Apart from the hadron groups of mesons $q\bar{q}$ and baryons qqq also exotic hadrons, e.g. tetraquarks $qq\bar{q}\bar{q}$, are possible in theory. QCD allows the formation of such states, because two quarks and two antiquarks can combine to a colour-singlet. Understanding exotic hadrons or to prove their existence or non-existence in case of tetraquarks is a long standing problem in particle physics.

1.1 Experimental tetraquark candidates

Observing exotic hadrons experimentally is much harder, than observing conventional mesons and baryons. For example, tetraquark candidates are elusive systems, high in the spectrum, which quickly decay to several non-exotic hadrons.

Several hadronic resonances, which are unconfirmed tetraquark candidates, are e.g. the light scalar mesons σ, κ, $f_0(980)$ and $a_0(980)$ and the heavier charm-strange mesons D^*_{s0} and D_{s1} [1, 2]. However, their quantum numbers and masses are not too different from what is expected in the $q\bar{q}$ picture and thus, it is not possible to find definite proof of their tetraquark nature.

The recently observed charmonium / bottomonium resonances $Z_c^{\pm}$ and $Z_b^{\pm}$ (among others by the BELLE collaboration [3, 4, 5]) are more obvious tetraquark candidates. Its masses and decay products give strong indications for hidden $c\bar{c}$ or $b\bar{b}$ pairs. But this alone can not explain the electrical charge.

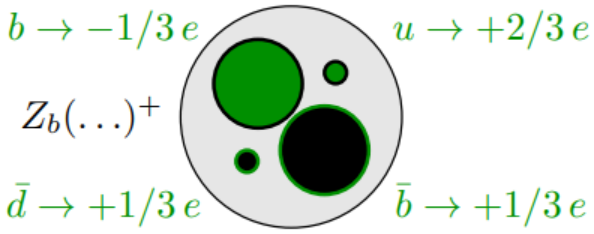

Figure 1.1: *Sketch of the charged bottomonium resonance $Z_b(10610)^+$ and $Z_b(10650)^+$ [35].*

Assuming a tetraquark structure, sketched in fig. 1.1 for the bottomonium resonance, solves this problem. In this case, the presence of a light quark and a light antiquark ($u \to +2/3e$ and $\bar{d} \to +1/3e$) is responsible for the charge ($Z_b(...) \equiv b\bar{b}u\bar{d}$). However, also for the $Z_b^{\pm}$ resonance, the tetra quark nature is disputable [6].

The discussed candidates, especially the charmonium resonance $Z_c^{\pm}$ have already received considerable experimental attention. Further measurements, aiming to learn more about the decay channels together with theoretical investigations can potentially clarify the status of these candidates in near future. The role of lattice QCD in this context is very important, since it can provide quantitative predictions, directly based on the QCD lagrangian, i.e. from first principles.

1.2 Tetraquarks from lattice QCD

Studying tetraquarks theoretically by means of lattice QCD is important to confirm and interpret corresponding experimental observations and as well to provide information in which channels tetraquarks may be found.

Due to the observations of $B^*\bar{B}$ and $B^*\bar{B}^*$ tetraquark candidates in experiments, it is desirable to investigate these systems also in theory. However, this is problematic because these they couple to at least five decay channels. Therefore it is convenient to concentrate first on the theoretically simpler BB systems. One can be optimistic, that after the observation of $B\bar{B}$ systems also BB tetraquarks may be observed in the near future in present day laboratories.

Furthermore, many technical difficulties concerning tetraquark studies can be avoided by searching for bound states rather than for resonances. This is appropriate, if the two involved antiquarks are sufficiently heavy (see Ref. [9] and the references therein). Considering two heavy antiquarks on the lattice in turn reduces the technical complexity of the four quark system, because they can be treated in leading order HQET, also known as static approximation, c.f. sec. 2.5. In this limit, the heavy quarks appear simply as static colour charges. Because the static approximation is most appropriate if the heavy (anti-)quarks are bottom (anti-)quarks, the term "static quark" can be seen as a synonym for the bottom quark from now on.

In the following, previous studies on which my thesis is based are introduced. Within the static-light approximation, the isospin, spin and parity dependent potential of a pair of B mesons was computed [9]. This is the first step in the Born-Oppenheimer approximation, which is used to find possibly existing tetraquark bound states. For a detailed introduction to this strategy, see Refs. [7, 8].

Born-Oppenheimer approximation:

1) Compute potentials of two static antiquarks $\bar{b}\bar{b}$ in the presence of two lighter quarks $qq \in \{ud, ss, cc\}$ using lattice QCD.

2) Check, whether these potentials are sufficiently attractive to host a bound state by solving a corresponding Schrödinger equation.

While there was no indication for a bound state for $qq \in \{ss, cc\}$, one bound state for the $\bar{b}\bar{b}ud$ tetraquark with quantum numbers $I(J^P) = 0(1^+)$ was found. The computations have been performed at three unphysically heavy pion masses, but the binding still survives after extrapolating down to the physical value. After including heavy spin effects [10], the binding energy of this state is $E_B = -59^{+38}_{-30}$ MeV.

More details about the work presented here, e.g. the hadron creation operators used for the numerical computations together with its characterizing quantum numbers are discussed in sec. 3.1.

It is worth to mention, that the bound $\bar{b}\bar{b}ud$ tetraquark state has also been predicted by other groups with the same quantum numbers, using a similar approach [11] and by a lattice computation with four quarks of finite mass [12].

1.3 Mesonic molecule vs. diquark-antidiquark

In this thesis, the previous studies about the bound $\bar{b}\bar{b}ud$ tetraquark state with quantum numbers $I(J^P) = 0(1^+)$ are extended. The goal is to investigate the internal structure of the predicted bound state. To this end, the mesonic molecule structure (BB) and the diquark-antidiquark structure (Dd) are compared to each other.

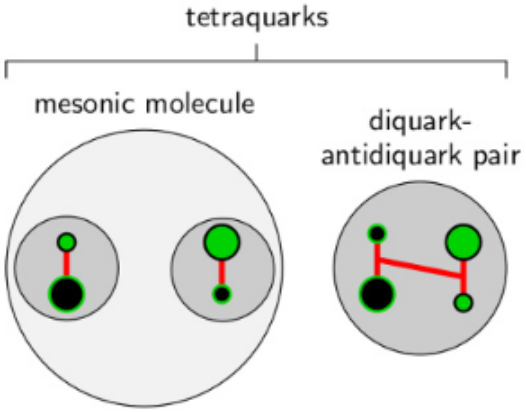

Figure 1.2: *Sketch of the mesonic molecule structure and the diquark-antidiquark structure [36].*

In fig. 1.2, both structures are illustrated. The mesonic molecule can be understood as two ordinary $\bar{q}q$ mesons, bound by residual strong forces, while in the diquark-antidiquark structure a diquark qq and an antidiquark $\bar{q}\bar{q}$ are strongly bound by a connecting flux tube of gluons. In sec. 3.1, differences and similarities of both structures are discussed based on their creation operators.

To analyze the internal tetraquark structure, we have to compute correlation matrices $C(t; r)$, containing both tetraquark structures for varying heavy quark separations r. Afterwards, the generalized eigenvalue problem (GEVP) has to be solved, with the correlation matrices as an input, c.f. sec. 2.6. From the resulting (ground state-) eigenvectors, the relative contributions of the different structures to the tetraquark ground state can be extracted as a function of the heavy antiquark separation. Moreover, the potential of the $\bar{b}\bar{b}$ pair in presence of light up and down quarks can be extracted from the eigenvalues, which also result from the solution of the GEVP, .

In the following, a short outline of this theses is given. The next chapter is about the theoretical foundations, e.g. key equations of lattice QCD and techniques to treat heavy quarks on the lattice are explained. Then, it is shown how the correlation matrices are constructed, based on the creation operators for the mesonic molecule and the diquark-antidiquark structure. Afterwards, the technical realization of the computation of the correlation matrix by means of lattice simulations is addressed. Following this, the results of the numerical computations are presented and explained. Finally, the last chapter summarizes the main findings of this theses and possible extensions for my work are proposed.

2 Theory

Lattice QCD is a powerful tool for calculations in in the low-energy regime of QCD, where perturbation theory is not applicable. In the following, key equations of lattice QCD, lattice actions for the gluons and fermions as well as special techniques, necessary to treat heavy quarks on the lattice are explained. Finally, the generalized eigenvalue problem and its use in the context of comparing tetraquark structures are discussed. For a more detailed and complete introduction to these topics, we want to refer to [33, 34] and / or to the references named in the following sections.

2.1 Notation

The Grassmann valued quark fields carry spin- and colour indices. The first is always denoted by a greek letter α, β, ... and the second by a roman letter a, b, ... Moreover, (f) indicates the quark flavour. Of course, the quark field depends on the space-time x. In our convention, quark fields of finite mass are denoted by Ψ and static quarks by Q. The static quarks are always bottom quarks here and don't need a flavour index.

$$\Psi^{(f)}(x)_{\ a}^{\alpha} \qquad Q(x)_{\ a}^{\alpha}$$

The gauge field also depends on the space-time x and furthermore on two colour indices (matrix in colour-space) and on a Lorentz index μ, which labels the direction of the different components in (euclidean) space-time.

$$A_\mu(x)_{ab}$$

Sometimes, the indices are omitted and matrix / vector notation is used instead.

We choose the chiral representation for the euclidean gamma matrices, c.f. sec. A.1. Finally, we note that we use natural units ($\hbar = c = 1$) and the sum convention, whenever the same Dirac- or colour index appears twice.

2.2 Key equations of lattice QCD

In lattice QCD, vacuum expectation values of physical observables are calculated as path integrals.

$$\langle O \rangle = \frac{1}{Z} \int \mathcal{D}[\Psi, \bar{\Psi}] \mathcal{D}[U] e^{-S_F[\Psi, \bar{\Psi}, U] - S_G[U]} O[\Psi, \bar{\Psi}, U] \tag{2.1}$$

Z is called partition function and is also expressed as path integral.

$$Z = \int \mathcal{D}[\Psi, \bar{\Psi}] \mathcal{D}[U] e^{-S_F[\Psi, \bar{\Psi}, U] - S_G[U]}$$

The (euclidean) QCD action was split up into two parts here, the fermionic action and the gauge action.

$$S_{QCD} = S_F[\Psi, \bar{\Psi}, U] + S_G[U]$$

Both actions are discussed in sec. 2.3 and sec. 2.4.

The integration variables in such path integrals are all involved quark- and gluon fields at all space-time points.

$$\mathcal{D}[\Psi,\bar{\Psi}] = \prod_{n\in\Lambda}\prod_{f,\alpha,c} d\Psi^{(f)}(n)_{\ c}^{\ \alpha}\ d\bar{\Psi}^{(f)}(n)_{\ c}^{\ \alpha}, \quad \mathcal{D}[U] = \prod_{n\in\Lambda}\prod_{\mu=1}^{4} dU_\mu(n)$$

$$\Lambda = \{n = (\boldsymbol{n}, n_4) \mid \boldsymbol{n} \in \Lambda_3,\ n_4 = 0, 1, \ldots, N_T - 1\}$$
$$\Lambda_3 = \{\boldsymbol{n} \mid n_i = 0, 1, \ldots, N - 1\}$$

The space-time lattice Λ was introduced at this point. The discretization is necessary to make the path integral mathematically well defined and numerically computable. It reduces the number of degrees of freedom in the path integral to a finite number. The lattice is also important in the context of regularization of QCD or other quantum field theories (lattice regularization).

The temporal and spacial extension of the lattice is given by the number of lattice points and the lattice spacing a, which separates two neighboring lattice points.

$$T = N_T \cdot a \qquad\qquad L = N \cdot a$$

By integrating out the Grassmann valued fermion fields, eq. 2.1 becomes

$$\langle O\rangle = \frac{1}{Z}\int \mathcal{D}[U]\prod_f \det(D_f[U])e^{-S_G[U]}O'[U]$$
$$Z = \int \mathcal{D}[U]\prod_f \det(D_f[U])e^{-S_G[U]}$$

$O'[U]$ denotes the observable after the integration, which typically consists of one or more fermion propagators and gauge transporters, which connecting spatially separated quarks. For each involved quark flavour f, also a corresponding fermion determinant $D_f[U]$ results from the integration.

The remaining integral over the gauge field is evaluated using a Monte-Carlo simulation. After N_{conf} gauge field configurations $\{U_i\}$ weighted by the factor $Z^{-1}\prod_f \det(D_f[U])e^{-S_G[U]}$ were generated, the expectation value can be evaluated according to

$$\langle O\rangle \approx \frac{1}{N_{conf}}\sum_{i=1}^{N_{conf}} O'(U_i)$$

Observables, which are considered in this thesis, are hadron creation operators. Let $O^\dagger(0)$ be the interpolator, which creates a particle with certain quantum numbers at time 0 and let $O(t)$ be the adjoint to this, which annihilates it at time t. Then, we can compare the expectation value $\langle O(t)O^\dagger(0)\rangle$, resulting from eq. 2.1 with the following alternative representation of it.

$$\begin{aligned}\lim_{T\to\infty}\langle O(t)O^\dagger(0)\rangle_T &= \sum_n \langle 0|\,\hat{O}\,|n\rangle\,\langle n|\,\hat{O}^\dagger\,|0\rangle\, e^{-tE_n}\\ &= \sum_n \left|\langle n|\,\hat{O}^\dagger\,|0\rangle\right|^2 e^{-tE_n}\end{aligned} \tag{2.2}$$

Here, E_n denote energy levels relative to the vacuum.

With this, we know how to extract the ground state energy of the hadron after having computed the expectation value of the observables. To this end, the expectation value, also referred to as correlation function, has to be evaluated for large euclidean times $t \to \infty$.

$$C(t) \equiv \lim_{T\to\infty} \langle O(t)O^\dagger(0)\rangle_T = \left|\langle p|\, \hat{O}_p^\dagger\, |0\rangle\right|^2 e^{-tE_p} + \underbrace{\left|\langle p'|\, \hat{O}_p^\dagger\, |0\rangle\right|^2 e^{-tE_p'}}_{\to 0} + \dots$$

The states $|p\rangle$, $|p'\rangle$ and energies E_p, $E_{p'}$ refer to the ground state and an excited state of the particle. All contributions, coming from higher energy levels vanish in the limit $t \to \infty$ and E_p can be extracted from the exponential decay of the correlation function.

$$m_{\text{eff}}(t) = \frac{1}{a}\log\Big(\frac{C(t)}{C(t+a)}\Big)$$

For large enough euclidean times, the effective mass is equal to the hadron ground state energy.

$$m_{\text{eff}}(t) \to E_p \quad \text{for} \quad t \to \infty$$

2.3 Gauge field on the lattice

Before a discretized action for the gauge field can be written down, the relation between the gauge field in the continuum $A_\mu(x)$ and the gauge link variables $U_\mu(n)$, $n \in \Lambda$, which live on the lattice has to be established.

The so-called gauge transporter is the path-ordered exponential integral of the gauge field A_μ along a curve $\mathcal{C}_{xy}$ connecting two points x and y.

$$G(x,y) = P\exp\Big(i\int_{\mathcal{C}_{xy}} A\cdot ds\Big)$$

The link variables are now defined as gauge transporter, which connects neighboring lattice points. For such a short distance, one can approximate the curve $\mathcal{C}_{xy}$.

$$U_\mu(n) = G(n, n+\hat{\mu}) = \exp(iaA_\mu(n)) = \mathbb{1} + iaA_\mu(n) + \mathcal{O}(a^2)$$

The most prominent lattice gauge action, expressed in terms of the link variables is called Wilson gauge action. It reads

$$S_G[U] = \frac{\beta}{3}\sum_{n\in\Lambda}\sum_{\mu<\nu}\text{Re}\ \text{tr}[\mathbb{1} - U_{\mu\nu}(n)] = \frac{a^4}{2g^2}\sum_{n\in\Lambda}\sum_{\mu,\nu}\text{tr}[F_{\mu\nu}(n)^2] + \mathcal{O}(a^2) \tag{2.3}$$

On the left side of this equation, the inverse coupling $\beta = 6/g^2$ was introduced. Within the definition of the Wilson gauge action, $U_{\mu\nu}(n)$ is the so-called plaquette.

$$U_{\mu\nu}(n) = U_\mu(n)U_\nu(n+\hat{\mu})U_\mu(n+\hat{\nu})^\dagger U_\nu(n)^\dagger$$

The plaquettes are the shortest, nontrivial closed loop on the lattice.

In the limit $a \to 0$, the Wilson gauge action is identical to the action in the continuum, as it was already indicated on the right side of eq. 2.3. If a is finite, we have to deal with discretization errors of $\mathcal{O}(a^2)$.

Eq. 2.3 is not the only discretized variant of the continuum gauge action. There are also other expressions for discretized lattice gauge actions, which also turn into the continuum action in the continuum limit. Different variants for the lattice action usually differ in their discretization errors. The gauge field configurations considered for the numerical computations in this theses were generated using the tree-level Symanzik improved action [13].

2.4 Fermions on the lattice

Wilson-fermions are one possibility to implement fermions on the lattice. The corresponding action reads

$$S_F[\Psi, \bar{\Psi}, U] = \sum_f a^4 \sum_{n,m \in \Lambda} \bar{\Psi}^{(f)}(n) D^{(f)}(n|m) \Psi^{(f)}(m) \tag{2.4}$$

with the Wilson Dirac operator

$$D^{(f)}(n|m)_{\substack{\alpha\beta \\ ab}} = \Big(m^{(f)} + \frac{4}{a}\Big)\delta_{\alpha\beta}\delta_{ab}\delta_{n,m} - \frac{1}{2a}\sum_{\mu=\pm 1}^{\pm 4}\Big(\mathbb{1} - \gamma_\mu\Big)_{\alpha\beta} U_\mu(n)_{ab}\delta_{n+\hat{\mu},m}$$

This action results from the so-called naive discretization by adding a term, which solves the doubling problem, i.e. removes unwanted poles from the fermion propagator. The discretization errors are of $\mathcal{O}(a)$.

However, for my calculations a modification of the Wilson-fermions was used, the Wilson twisted mass fermions. A detailed introduction to twisted mass lattice QCD can be found in [14]. This section is meant to give a brief overview.

The Wilson twisted mass action for two mass degenerate light quark flavours ($N_f = 2$) reads

$$S_F^{tw}[\chi, \bar{\chi}, U] = a^4 \sum_{k,n \in \Lambda} \bar{\chi}(k) \underbrace{\Big(D(k|n)\mathbb{1}_2 + m\mathbb{1}_2\delta_{k,n} + i\mu\gamma_5\tau_3\delta_{k,n}\Big)}_{D(k|n)_{tw}} \chi(n) \tag{2.5}$$

Within the definition of the twisted basis Dirac operator $D(k|n)_{tw}$, the massless ($m = 0$) Wilson Dirac operator $D(k|n)$ appears.

Along with spin- and colour indices, the spinors $\bar{\chi}$ and χ also carry a flavour index, i.e. we note

$$\chi = \begin{pmatrix} \chi^{(u)} \\ \chi^{(d)} \end{pmatrix}$$

The action 2.5 differs from eq. 2.4 for two mass degenerate flavours by adding the twisted mass term $i\mu\gamma_5\tau^3$ to the Dirac operator. The real parameter μ is called twisted mass. This term is trivial only in colour space, has a γ_5 in Dirac space and the third Pauli matrix $\tau_3 = \mathrm{diag}(1, -1)$ acts in flavour space.

The fermion fields in the twisted basis χ are related to the fermions in (pseudo) physical basis via the twist rotation.

$$\Psi = e^{i\omega\gamma_5\tau_3/2}\chi, \quad \bar{\Psi} = \bar{\chi}e^{i\omega\gamma_5\tau_3/2} \tag{2.6}$$

In Refs. [15, 16], it was shown that twisted mass formulation is equivalent to the standard QCD in the continuum. On the lattice, we can profit from the automatic $\mathcal{O}(a)$ improvement, if the twist angle is tuned to maximal twist $\omega = \pi/2$.

Another advantage of this action is, that we don't have to worry about exceptional configurations, because the determinant of the twisted mass Dirac operator is real and strictly positive for arbitrary gauge configurations, as long as $\mu \neq 0$.

The price to pay is the breaking of parity and isospin symmetries on the lattice. However, this breaking is only an $\mathcal{O}(a^2)$ discretization effect (at maximal twist), i.e. the symmetries are restored in the continuum. From this, it follows that isospin I is not a quantum number, only I_z is conserved. Consequently, mixing between the continuum sectors ($I = 0$, $I_z = 0$) and ($I = 1$, $I_z = 0$) can occur.

Further properties of the twisted mass formulation are discussed in sec. 3 and sec. 4.4, e.g. the twisted mass quantum numbers and symmetries of the twisted basis propagator.

2.5 Heavy Quark Effective Theory (HQET)

Treating bottom (anti-)quarks fully dynamically on present days lattices is not possible, because their mass is larger than the realizable lattice cutoff. An effective theory for heavy quarks has to be considered. This will lead us to the static approximation at the end of this section.

In HQET, the central idea is to scale out the trivial contribution to hadron masses, when heavy quarks are involved, which is the mass of the heavy valence quark m_h itself. This would result in an considerable reduction of the energy scale of the problem. Using the Foldy-Wouthuysen transformation leads to an expansion of the action for the heavy flavours in terms of $1/m_h$ [33].

$$\bar{q}(\gamma_\mu D_\mu + m_h)q \quad \rightarrow \quad \underbrace{\bar{\Psi}_h\Big(m_h + D_0\Big)\Psi_h}_{\mathcal{L}_h^{stat}} + \mathcal{O}(1/m_h)$$

D_0 denotes the time component of the covariant derivative $D_\mu = \partial_\mu + iA_\mu$. The spinors $q, \bar{q}$ describing the relativistic quarks on the left side of the equation were replaced by projected, non-relativistic spinors Ψ_h, $\bar{\Psi}_h$, which obey

$$P_+\Psi_h = \Psi_h, \quad \bar{\Psi}_h P_+ = \bar{\Psi}_h, \quad P_+ = \frac{\mathbb{1} + \gamma_0}{2}$$

In this work, we treat the heavy antiquarks in leading order HQET, i.e. we neglect effects $\mathcal{O}(1/m_h)$. For the bottom antiquark, this approximation is appropriate. In this case, propagation is only possible in time direction, but not in space. This is why this approximation is called static approximation. This scenario would be exact, if the quark was infinitely heavy,

i.e. $m_h \to \infty$.

The analogue of the static action on the lattice is called Eichten-Hill action und is defined as follows [17].

$$S_h = a^4 \frac{1}{1 + a\delta m_h} \sum_{n \in \Lambda} \bar{\Psi}_h(n) \Big(\delta m_h + \tilde{\nabla}_0 \Big) \Psi_h(n)$$

where $\tilde{\nabla}_0$ denotes the covariant derivative in time direction.

$$\tilde{\nabla}_0 \Psi_h(n) \equiv \frac{1}{a} [\Psi_h(n) - U_0^\dagger(n - \hat{0}) \Psi_h(n - \hat{0})]$$

The heavy quark propagator $G_Q(x, y)$, which obeys

$$(\delta m_h + \tilde{\nabla}_0) G_Q(x, y) = \delta(x - y) P_+$$

reads ($a\delta \hat{m}_h = \ln(1 + a\delta m_h)$) [18, 19]

$$G_Q(x, y) = \Theta(x_0 - y_0)\ \delta(\vec{x} - \vec{y})\ \exp(-\delta \hat{m}_h (x_0 - y_0))\ U(\vec{x}, x_0; \vec{y}, y_0)\ (\frac{\mathbb{1} + \gamma_0}{2}) \tag{2.7}$$

From this it can be seen, that (infinitely) heavy quarks appear simply as colour source.

Eq. 2.7 describes the propagation of a static quark. Analogous to this, the static antiquark propagator can be derived und both results can be summarized in one equation using the theta function.

$$\begin{aligned} G_Q(x, y) = \delta(\vec{x} - \vec{y}) \underbrace{U(x, y)}_{HYP2} \Big(& \Theta(y_0 - x_0)\ (\frac{\mathbb{1} - \gamma_0}{2})\ \exp(-\delta \hat{m}_h (y_0 - x_0)) \\ & + \Theta(x_0 - y_0)\ (\frac{\mathbb{1} + \gamma_0}{2})\ \exp(-\delta \hat{m}_h (x_0 - y_0)) \Big) \end{aligned} \tag{2.8}$$

$U(x, y)$ denotes the path ordered product of links along the straight line from x to y. The static propagators enter the correlation functions with HYP2 smeared link variables. This has been found to be useful in improving the signal to noise ratio in static-light correlation functions. In Ref. [9], a comparison of lattice potentials with and without the use of HYP2 smearing in the static quark propagators can be found. Strictly speaking, the static quark propagator in eq. 2.8 is not any more the propagator corresponding to the Eichten-Hill action, because this is only defined with ordinary (unsmeared) link variables. The corresponding action is called HYP2 static action in this case.

2.6 Generalized eigenvalue problem (GEVP)

Again, this section is meant as short overview. For a more detailed discussion of the GEVP, the reader is refered to [20].

The generalized eigenvalue problem is defined as follows.

$$C(t) v_n(t, t_0) = \lambda_n(t, t_0) C(t_0) v_n(t, t_0), \quad n = 0, \ldots, N - 1, \quad t > t_0$$

The correlation matrix $C(t)$

$$C_{ij}(t) = \langle \mathcal{O}_i(t) \mathcal{O}_j^\dagger(0) \rangle = \sum_n \langle 0| \hat{O}_i |n\rangle \langle n| \hat{O}_j^\dagger |0\rangle e^{-tE_n}, \quad i,j = 1,\dots,N$$

has to be computed by means of lattice QCD and enters the GEVP as an input. The dimension N of the correlation matrix is the number of the different considered states. In this thesis, two different tetraquark structures (carrying the same quantum numbers) are considered. After having solved the GEVP, two different output values $\lambda_n(t,t_0)$ and $v_n(t,t_0)$ are available to us.

The eigenvalues $\lambda_n(t,t_0)$ allow to determine the ground state energy as well as excited states ($n = 0,\dots,N-1$) according to

$$E_n = \lim_{t\to\infty} E_n^{\text{eff}}(t,t_0), \quad E_n^{\text{eff}}(t,t_0) \equiv \frac{1}{a} \log \frac{\lambda_n(t,t_0)}{\lambda_n(t+a,t_0)}$$

It is known, that the convergence of the effective mass to a specific energy levels is better, if no other energy level is close to the desired one.

$$E_n^{\text{eff}}(t,t_0) = E_n + \mathcal{O}(e^{-\Delta E_n t}), \quad \Delta E_n = \min_{m\neq n} |E_m - E_n|$$

The eigenvectors $v_n(t,t_0)$ provide information about the internal structure of the four-quark system. Since we are interested in the structure of the tetraquark ground state, $v_0(t,t_0)$ is most important to us. Related to my work, the eigenvector entries are the coefficients in the expansion of the $\bar{b}\bar{b}ud$ tetraquark state in terms of the BB and Dd states.

$$|\bar{b}\bar{b}ud\rangle \approx \sum_j v_0^j(t,t_0) \mathcal{O}_j^\dagger |0\rangle, \quad j \in \{BB, Dd\} \tag{2.9}$$

Here, "$\approx$" denotes the expansion in the "$\mathcal{O}_{BB}$ $\mathcal{O}_{Dd}$" subspace. Of course, only structures which are contained in the computed correlation matrix can contribute to the state in eq. 2.9. Thus, the entries in the eigenvectors should not be understood as definite contributions, but rather as the relative weight compared only to the other considered structures.

3 Entries of the correlation matrix

This section is about the creation operators for the mesonic molecule (BB) and the diquark-antidiquark (Dd) tetraquark structures, which are used in the numerical calculations and the resulting correlation functions. Deriving the correlation functions based on the creation operators is straightforward and thus, for the sake of clarity only final results for this calculations are shown and possible intermediate steps, c.f. sec. A.2 for example, are omitted. Moreover, the connection to previous studies of the BB systems is established in this context, which have led to the prediction of a bound $\bar{b}\bar{b}ud$ tetraquark state with quantum numbers $I(J^P) = 0(1^+)$.

3.1 Diagonal entries

By definition, the correlation matrix

$$C_{ij}(t) = \langle \mathcal{O}_i(t)\mathcal{O}_j^\dagger(0)\rangle, \quad i,j \in \{BB, Dd\} \tag{3.1}$$

is hermitian and thus, the diagonal entries $\langle \mathcal{O}_{BB}(t)\mathcal{O}_{BB}^\dagger(0)\rangle$ and $\langle \mathcal{O}_{Dd}(t)\mathcal{O}_{Dd}^\dagger(0)\rangle$ are real and from eq. 2.2 we also know, that they are positive.

Mesonic molecule

First, the mesonic molecule (BB) creation operator and its quantum numbers are discussed. It reads ($C = \gamma_0\gamma_2$ is the charge conjugation matrix)

$$\mathcal{O}_{BB}(t) = (C\Gamma)_{\alpha\beta}\ (C\tilde{\Gamma})_{\gamma\delta}\ (\bar{Q}_{\substack{\gamma\\ a}}(\vec{r}_1,t)\ \Psi^{(f)}_{\substack{\alpha\\ a}}(\vec{r}_1,t))\ (\bar{Q}_{\substack{\delta\\ b}}(\vec{r}_2,t)\ \Psi^{(f')}_{\substack{\beta\\ b}}(\vec{r}_2,t))$$

This interpolator describes a pair of (static-light) B mesons, which are spatially separated by $r = |\vec{r}_2 - \vec{r}_1|$. To be more precise, only the position of the static antiquarks is fixed, while the light quarks form a cloud around them. Without loss of generality, the z-axis is chosen to be the axis of separation for the heavy quarks. The BB states can be labeled by five different quantum numbers [9].

- Isospin $I \in \{0,1\}$ and its z-component $I_z \in \{-1,0,1\}$.
- Absolute value of the z-component of the light quark spin $|j_z| \in \{0,1\}$. Since heavy quark spin effects are absent in leading order HQET, it is sufficient to consider only the relativistic spin as label.
- Eigenvalue of the parity operator $\mathcal{P} \in \{+,-\}$.
- Reflections across the x-axis, $\mathcal{P}_x \in \{+,-\}$.

The isospin quantum numbers I, I_z depend on the flavour combination.

- $\Psi^{(f)}\Psi^{(f')} = (ud - du)/\sqrt{2}$ with $I = 0$.
- $\Psi^{(f)}\Psi^{(f')} = uu$ with $I = 1, I_z = 1$.
- $\Psi^{(f)}\Psi^{(f')} = dd$ with $I = 1, I_z = -1$.
- $\Psi^{(f)}\Psi^{(f')} = (ud + du)/\sqrt{2}$ with $I = 1, I_z = 0$.

The remaining three quantum numbers $|j_z|, \mathcal{P}, \mathcal{P}_x$ depend on the choice for the spin matrix Γ. The quantum numbers for the BB systems are collected in tab. A.2. The trial states in twisted basis χ are related to the trial states in physical basis Ψ via the twist rotation, c.f. eq. 2.6.

$$\begin{aligned}\mathcal{O}_{BB}(t) &= (C\Gamma)_{\alpha\beta}\ (C\tilde{\Gamma})_{\gamma\delta}\ (\bar{Q}_{\ a}^{\gamma}(\vec{r}_1,t)\ (e^{\pm i\frac{\omega}{2}\gamma_5})_{\alpha\mu}\ \chi_{\mu\ a}^{(f)}(\vec{r}_1,t))\ (\bar{Q}_{\ b}^{\delta}(\vec{r}_2,t)\ (e^{\mp i\frac{\omega}{2}\gamma_5})_{\beta\nu}\ \chi_{\nu\ b}^{(f')}(\vec{r}_2,t)) \\ &= \underbrace{(e^{\pm i\frac{\omega}{2}\gamma_5})_{\mu\alpha}\ (C\Gamma)_{\alpha\beta}\ (e^{\mp i\frac{\omega}{2}\gamma_5})_{\beta\nu}}_{(C\Gamma_{tm})}\ (C\tilde{\Gamma})_{\gamma\delta}\ (\bar{Q}_{\ a}^{\gamma}(\vec{r}_1,t)\ \chi_{\mu\ a}^{(f)}(\vec{r}_1,t))\ (\bar{Q}_{\ b}^{\delta}(\vec{r}_2,t)\ \chi_{\nu\ b}^{(f')}(\vec{r}_2,t))\end{aligned}$$

We see, that transforming the light quark propagators in the physical basis into the quark propagators in the twisted basis is effectively done by redefining the spin matrices according to

$$\begin{aligned}(e^{+i\frac{\omega}{2}\gamma_5})(C\Gamma)(e^{-i\frac{\omega}{2}\gamma_5}) &= C\Gamma_{tm}^{(+-)} \\ (e^{-i\frac{\omega}{2}\gamma_5})(C\Gamma)(e^{+i\frac{\omega}{2}\gamma_5}) &= C\Gamma_{tm}^{(-+)}\end{aligned}$$

The right hand side of these two equations defines the spin-matrices in the twisted basis, $\Gamma_{tm}^{(+-)}$ and $\Gamma_{tm}^{(-+)}$. As shown above, the twisted basis spin matrices Γ_{tm} depend on the flavour combination in the creation operator. In this thesis, only correlation functions with the $(ud-du)/\sqrt{2}$ flavour combination are computed. Therefore, the twist rotation matrices will always differ in their sign and knowledge about Γ_{tm}^{++} or Γ_{tm}^{--} is not necessary.

In tab. A.3, the quantum numbers are collected again for $\chi^{(f)}\chi^{(f')} = ud \pm du$, where $\mathcal{P}^{(tm)} \equiv \mathcal{P} \times [u \leftrightarrow d]$ and $\mathcal{P}_x^{(tm)} \equiv \mathcal{P}_x \times [u \leftrightarrow d]$ denote the twisted mass counterparts of parity and reflection across the x-axis.

Also in [9], it was shown that the BB states are not fully characterized by their quantum numbers. One can also express the BB systems in terms of individual B mesons. The relation between the physical basis spin structure and the static-light meson content can be seen in tab. A.1. In this notation, S denotes a B meson with quantum numbers $J^P = 0^-$ ($B^\pm$ or B^0) or $J^P = 1^-$ (B^*) [2]. These mesons are degenerate in the static limit. P_- corresponds to B_0^* with $J^P = 0^+$ or B_1^* with $J^P = 1^+$ [21, 22].

After having computed the isospin, spin and parity (and meson content) dependent lattice potentials of the B meson pairs, it is possible to determine if a bound state arises, using the Born-Oppenheimer perspective, c.f. sec. 1.2. The result of this studies is, that there is strong indication for binding in the spin/isospin singlet, which is the multiplet A in tab. A.3, with $\Gamma = (1+\gamma_0)\gamma_5$ (pb) and flavour structure $(ud-du)/\sqrt{2}$. The corresponding potential has twice the mass of the S meson as asymptotic value. This is in accordance with tab. A.1, where the cancellation of P_- mesons can be explained.

In Refs. [8, 35], the quantum numbers of the predicted tetraquark bound state are discussed. Isospin $I = 0$ comes from the flavour combination $(ud-du)/\sqrt{2}$, the heavy quark spin $j_b = 1$ is responsible for total spin $J = 1$ and the parity $P = +$ is the product of the parity quantum numbers of the two B mesons, which are both negative.

The main goal of this thesis is to investigate the internal structure of this possibly existing tetraquark. To this end, we have to compute correlation functions for different structures with the above discussed quantum numbers, corresponding to the $(ud - du)/\sqrt{2}$ flavour combination and $\Gamma = (1+\gamma_0)\gamma_5$ (pb). Tab. 3.1 shows the relation between Γ and Γ_{tm} for this choice (at maximal twist $\omega = \pi/2$).

Γ	$\Gamma_{tm}^{(+-)}$	$\underset{tm}{(-+)}$
γ_5	$+\gamma_5$	$+\gamma_5$
$\gamma_0\gamma_5$	$-i\gamma_0$	$+i\gamma_0$

Table 3.1: *Relation between Γ in physical basis and the corresponding Γ_{tm} in twisted basis. See also tab. A.3*

Deriving the correlation function for the mesonic molecule structure based on the creation operator is straightforward. The first step is to integrate out the fermions in the path integral, eq. 2.1. This results in the static quark propagators (c.f. eq. 2.8) and light quark propagators, denoted by $G^{(u/d)}(\vec{r}_1, t_1|\vec{r}_2, t_2)$. The static approximation simplifies this calculation at this point, because further Wick contractions, that would appear and propagate the heavy quarks also in space vanish. The remaining integration over the gauge field is denoted by $\langle ... \rangle$.

$$
\begin{aligned}
&\langle 0|\, \mathcal{O}_{BB}(t)\mathcal{O}^{\dagger}_{BB}(0)\,|0\rangle\,|_{I=0} \propto \\
&+ (C\Gamma^{+-}_{tm})_{\alpha\beta}\ (\gamma_0(C\Gamma^{+-}_{tm})^{\dagger}\gamma_0)_{\mu\nu} \\
&\underbrace{\langle [U(\vec{r}_1,0;\vec{r}_1,t)_{ca}\ G^{(u)}(\vec{r}_1,t|\vec{r}_1,0)^{\ \alpha\nu}_{ac}]\ [U(\vec{r}_2,0;\vec{r}_2,t)_{db}\ G^{(d)}(\vec{r}_2,t|\vec{r}_2,0)^{\ \beta\mu}_{bd}]\rangle}_{C_{11}^{(1)}} \\
&+ (C\Gamma^{+-}_{tm})_{\alpha\beta}\ (\gamma_0(C\Gamma^{-+}_{tm})^{\dagger}\gamma_0)_{\mu\nu} \\
&\underbrace{\langle [U(\vec{r}_1,0;\vec{r}_1,t)_{ca}\ G^{(u)}(\vec{r}_1,t|\vec{r}_2,0)^{\ \alpha\mu}_{ad}\ U(\vec{r}_2,0;\vec{r}_2,t)_{db}\ G^{(d)}(\vec{r}_2,t|\vec{r}_1,0)^{\ \beta\nu}_{bc}]\rangle}_{C_{11}^{(2)}} \\
&+ (C\Gamma^{-+}_{tm})_{\alpha\beta}\ (\gamma_0(C\Gamma^{+-}_{tm})^{\dagger}\gamma_0)_{\mu\nu} \\
&\underbrace{\langle [U(\vec{r}_1,0;\vec{r}_1,t)_{ca}\ G^{(d)}(\vec{r}_1,t|\vec{r}_2,0)^{\ \alpha\mu}_{ad}\ U(\vec{r}_2,0;\vec{r}_2,t)_{db}\ G^{(u)}(\vec{r}_2,t|\vec{r}_1,0)^{\ \beta\nu}_{bc}]\rangle}_{C_{11}^{(3)}} \\
&+ (C\Gamma^{-+}_{tm})_{\alpha\beta}\ (\gamma_0(C\Gamma^{-+}_{tm})^{\dagger}\gamma_0)_{\mu\nu} \\
&\underbrace{\langle [U(\vec{r}_1,0;\vec{r}_1,t)_{ca}\ G^{(d)}(\vec{r}_1,t|\vec{r}_1,0)^{\ \alpha\nu}_{ac}]\ [U(\vec{r}_2,0;\vec{r}_2,t)_{db}\ G^{(u)}(\vec{r}_2,t|\vec{r}_2,0)^{\ \beta\mu}_{bd}]\rangle}_{C_{11}^{(4)}}
\end{aligned}
\tag{3.2}
$$

We write "$\propto$" because an overall factor K was neglected for better readability.

$$K = \frac{\exp(-2\delta\hat{m}_h t)}{2}\,\mathrm{tr}\{(\frac{\mathbb{1}-\gamma_0}{2})(C\tilde{\Gamma})(\frac{\mathbb{1}-\gamma_0}{2})(\gamma_0(C\tilde{\Gamma})^{\dagger}\gamma_0)\}$$

Due to the isospin combination $(ud-du)/\sqrt{2}$, four contributions (diagrams) to the correlation function arise. Their diagrammatic representations are shown in fig. 3.1. The horizontal axis

represents the heavy quark separation r and the time t is developing in vertical direction. The large, black circles represent static antiquarks. Their propagation (only in time direction) is shown as a black thick line. Light quarks and light quark propagators are represented by coloured circles and coloured lines, where the different colours distinguish between the light quark flavours (up/down). The diagrams for $C_{11}^{(1)}$ and $C_{11}^{(4)}$ can be found on the left hand side in fig. 3.1. The diagrams for $C_{11}^{(2)}$ and $C_{11}^{(3)}$ on the right hand side are called cross diagrams because the light quarks swap their positions. Diagrams $C_{11}^{(1)}/C_{11}^{(4)}$ and $C_{11}^{(2)}/C_{11}^{(3)}$ are exactly the same, but with interchanged quark flavours.

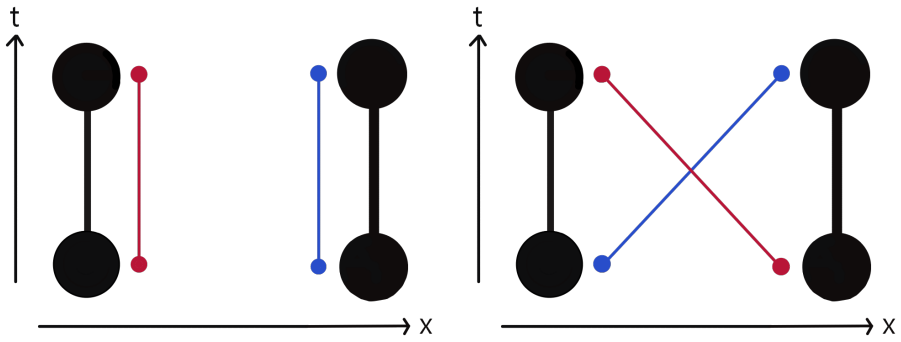

Figure 3.1: *Diagrams $C_{11}^{(1)}/C_{11}^{(4)}$ (lhs) and $C_{11}^{(2)}/C_{11}^{(3)}$ (rhs).*

The spin matrix $\tilde{\Gamma}$, which combines the heavy quarks, has to be chosen such that the trace

$$\{(\frac{\mathbb{1}-\gamma_0}{2})(C\tilde{\Gamma})(\frac{\mathbb{1}-\gamma_0}{2})(\gamma_0(C\tilde{\Gamma})^\dagger\gamma_0)\}$$

is unequal zero. This is only possible for $\tilde{\Gamma} = \{(1+\gamma_0)\gamma_5, (1+\gamma_0)\gamma_j\}$, $j = 1,2,3$. Since the trace over the heavy spin matrices is just a constant number for appropriate choices, the potentials are completely independent of the heavy quark spin effects, which is understandable in the context of leading order HQET.

Although from the numerical point of view one can not distinguish between $\tilde{\Gamma} = (1+\gamma_0)\gamma_5$ and $\tilde{\Gamma} = (1+\gamma_0)\gamma_j$, $j = 1,2,3$, the first of these two options can be ruled out. As mentioned above, we know that the heavy quark spin is $j_b = 1$ for the bound state.

For $\tilde{\Gamma} = (1+\gamma_0)\gamma_5$, we find

$$(C\tilde{\Gamma})^T = -(C\tilde{\Gamma})$$

while for $\tilde{\Gamma} = (1+\gamma_0)\gamma_j$, $j = 1,2,3$, we obtain

$$(C\tilde{\Gamma})^T = +(C\tilde{\Gamma})$$

Only the symmetrical spin alignment can lead to $j_b = 1$.

Diquark-Antidiquark

The creation operator for the diquark-antidiquark (Dd) state in twisted basis reads

$$\begin{aligned}\mathcal{O}_{Dd}(t) =&(C\Gamma_{tm})_{\alpha\beta}\ (C\tilde{\Gamma})_{\gamma\delta}\ \Big(\chi^{(f)}_{\substack{\alpha\\a}}(\vec{z},t)\ \chi^{(f')}_{\substack{\beta\\b}}(\vec{z},t)\ \epsilon_{abc}\Big)\\ &\Big(\epsilon_{cde}\ \bar{Q}_{\substack{\gamma\\f}}(\vec{r}_1,t)\ U(\vec{r}_1,t;\vec{z},t)_{fd}\ \bar{Q}_{\substack{\delta\\g}}(\vec{r}_2,t)\ U(\vec{r}_2,t;\vec{z},t)_{ge}\Big)\end{aligned}$$

On the first view, it becomes clear that the BB and Dd creation operators differ in their colour structures and in the positioning of the light quarks (c.f. fig. 3.1 and fig. 3.2). Their spin structure is however identical. This operator describes a (static) spatially extended antidiquark, expected to be in a colour triplet [3] in case of a bound tetraquark state, which combines with a relativistic diquark at position $\vec{z}$ in a colour antitriplet $[\bar{3}]$ to a colour-singlet. Position $\vec{z}$ is always chosen such, that it is exactly in the middle of the connecting line of the static quarks.

In this structure, the heavy antiquarks $\bar{Q}(\vec{r}_1,t)$ / $\bar{Q}(\vec{r}_2,t)$ are connected to the spatially separated light diquark via gauge transporters $U(\vec{r}_1,t;\vec{z},t)$ / $U(\vec{r}_2,t;\vec{z},t)$. In this case, increasing the heavy quark separation obviously means to separate colour charge and to enlarge the connecting product of links. According to the discussion in sec. 1.3, this corresponds to extending the flux tube of gluons, which connects the diquark and the antidiquark. From the point of view of formation of tetraquark states, this is clearly unfavorable compared to the mesonic molecule state. It is expected, that the overlap of the diquark-antidiquark operator with the tetraquark ground state gets worse for growing heavy quarks separations.

In comparison to the mesonic molecule correlation function, the flavour-combination, corresponding to $I = 0$ can be problematic in this case.

$$\begin{aligned}&\frac{1}{\sqrt{2}}\Big(\chi^{(u)}_{\substack{\alpha\\a}}(\vec{z},t)\ (C\Gamma^{+-}_{tw})_{\alpha\beta}\ \chi^{(d)}_{\substack{\beta\\b}}(\vec{z},t)\ \epsilon_{abc} - \chi^{(d)}_{\substack{\alpha\\a}}(\vec{z},t)\ (C\Gamma^{-+}_{tw})_{\alpha\beta}\ \chi^{(u)}_{\substack{\beta\\b}}(\vec{z},t)\ \epsilon_{abc}\Big)\\ =&\frac{1}{\sqrt{2}}\ \chi^{(u)}_{\substack{\alpha\\a}}(\vec{z},t)\ \Big((C\Gamma^{+-}_{tw})_{\alpha\beta} - (C\Gamma^{-+}_{tw})^T_{\alpha\beta}\Big)\chi^{(d)}_{\substack{\beta\\b}}(\vec{z},t)\ \epsilon_{abc}\end{aligned} \tag{3.3}$$

From this lines, we learn that for the diquark-antidiquark operator chosen here, $I = 0$ is not possible for arbitrary spin matrices Γ, corresponding to specific quantum numbers. Only Γ, obeying the relation $(C\Gamma^{-+}_{tw})^T \neq (C\Gamma^{+-}_{tw})$ are allowed, otherwise the operator would vanish. $\Gamma = (1+\gamma_0)\gamma_5$ is a suitable choice, because here we have $(C\Gamma^{-+}_{tw})^T = -(C\Gamma^{+-}_{tw})$. With this, eq. 3.3 becomes

$$\sqrt{2}\ \chi^{(u)}_{\substack{\alpha\\a}}(\vec{z},t)\ (C\Gamma^{+-}_{tw})_{\alpha\beta}\ \chi^{(d)}_{\substack{\beta\\b}}(\vec{z},t)\ \epsilon_{abc}$$

For a suitable Γ, the $I = 0$ correlation function for die diquark-antidiquark reads (propor-

tionality factor $4K$)

$$\begin{aligned}
&\langle 0|\, \mathcal{O}_{Dd}(t)\mathcal{O}^{\dagger}_{Dd}(0)\,|0\rangle \propto \\
&+ (C\Gamma^{+-}_{tw})_{\alpha\beta}\ (\gamma_0(C\Gamma^{+-}_{tw})^{\dagger}\gamma_0)_{\mu\nu}\ \underbrace{\langle [M^{(u)}(\vec{z},\vec{r}_1)\,{}^{\alpha\nu}_{aa}]\ [M^{(d)}(\vec{z},\vec{r}_2)\,{}^{\beta\mu}_{bb}]\rangle}_{C_{22}^{(1)}} \\
&- (C\Gamma^{+-}_{tw})_{\alpha\beta}\ (\gamma_0(C\Gamma^{+-}_{tw})^{\dagger}\gamma_0)_{\mu\nu}\ \underbrace{\langle [M^{(u)}(\vec{z},\vec{r}_1)\,{}^{\alpha\nu}_{ab}\ M^{(d)}(\vec{z},\vec{r}_2)\,{}^{\beta\mu}_{ba}]\rangle}_{C_{22}^{(2)}} \\
&- (C\Gamma^{+-}_{tw})_{\alpha\beta}\ (\gamma_0(C\Gamma^{+-}_{tw})^{\dagger}\gamma_0)_{\mu\nu}\ \underbrace{\langle [M^{(u)}(\vec{z},\vec{r}_2)\,{}^{\alpha\nu}_{ab}\ M^{(d)}(\vec{z},\vec{r}_1)\,{}^{\beta\mu}_{ba}]\rangle}_{C_{22}^{(3)}} \\
&+ (C\Gamma^{+-}_{tw})_{\alpha\beta}\ (\gamma_0(C\Gamma^{+-}_{tw})^{\dagger}\gamma_0)_{\mu\nu}\ \underbrace{\langle [M^{(u)}(\vec{z},\vec{r}_2)\,{}^{\alpha\nu}_{aa}]\ [M^{(d)}(\vec{z},\vec{r}_1)\,{}^{\beta\mu}_{bb}]\rangle}_{C_{22}^{(4)}}
\end{aligned} \tag{3.4}$$

with

$$M^{(x)}(\vec{z},\vec{v})\,{}^{\alpha\beta}_{ab} = U(\vec{z},0;\vec{v},0)_{ac}\ U(\vec{v},0;\vec{v},t)_{cd}\ U(\vec{v},t;\vec{z},t)_{de}\ G^{(x)}(\vec{z},t|\vec{z},0)\,{}^{\alpha\beta}_{eb}$$

In the diquark-antidiquark state, the colour structure is responsible for the emergence of four diagrams instead of the flavour combination, because here the two levi-civita tensors coming from the creation operator and two more coming from the annihilation operator are combined in the following way.

$$\begin{aligned}
(\epsilon_{abc}\epsilon_{cde})(\epsilon_{hij}\epsilon_{jmn}) &= (\delta_{ad}\delta_{be} - \delta_{ae}\delta_{bd})(\delta_{hm}\delta_{in} - \delta_{hn}\delta_{im}) \\
&= \delta_{ad}\delta_{be}\delta_{hm}\delta_{in} - \delta_{ad}\delta_{be}\delta_{hn}\delta_{im} - \delta_{ae}\delta_{bd}\delta_{hm}\delta_{in} + \delta_{ae}\delta_{bd}\delta_{hn}\delta_{im}
\end{aligned}$$

In fig. 3.2, the diagrammatic representation of the diquark-antidiquark correlation function is shown. Again, $C_{22}^{(1)}/C_{22}^{(4)}$ and $C_{22}^{(2)}/C_{22}^{(3)}$ differ only by the exchange of the light quark flavours. The grey and the black area on the left hand side indicate two different traces in colour space ($\vec{z} \to \vec{r}_1 \to \vec{z}$ and $\vec{z} \to \vec{r}_2 \to \vec{z}$) while on the right hand side a single trace is taken over the whole diagram.

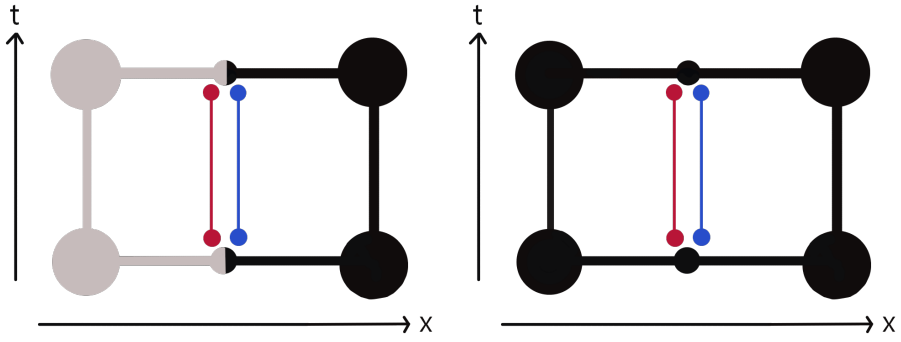

Figure 3.2: *Diagrams $C_{22}^{(1)}/C_{22}^{(4)}$ (lhs) and $C_{22}^{(2)}/C_{22}^{(3)}$ (rhs).*

If the heavy quarks are not separated, we find ($\vec{r}_1 = \vec{r}_2 = \vec{z}$)

$$\begin{aligned}
\mathcal{O}_{Dd}(t)|_{r=0} =& (C\Gamma_{tm})_{\alpha\beta}\ (C\tilde{\Gamma})_{\gamma\delta}\ \Big(\chi^{(f)}_{\substack{\alpha\\ a}}(\vec{z},t)\ \chi^{(f')}_{\substack{\beta\\ b}}(\vec{z},t)\ \epsilon_{abc}\Big) \\
&\Big(\epsilon_{cde}\ \bar{Q}_{\substack{\gamma\\ f}}(\vec{z},t)\ \underbrace{U(\vec{z},t;\vec{z},t)_{fd}}_{\delta_{fd}}\ \bar{Q}_{\substack{\delta\\ g}}(\vec{z},t)\ \underbrace{U(\vec{z},t;\vec{z},t)_{ge}}_{\delta_{ge}}\Big) \\
=& (C\Gamma_{tm})_{\alpha\beta}\ (C\tilde{\Gamma})_{\gamma\delta}\ \Big(\chi^{(f)}_{\substack{\alpha\\ a}}(\vec{z},t)\ \chi^{(f')}_{\substack{\beta\\ b}}(\vec{z},t)\Big)\ \Big(\bar{Q}_{\substack{\gamma\\ d}}(\vec{z},t)\ \bar{Q}_{\substack{\delta\\ e}}(\vec{z},t)\Big)(\delta_{ad}\delta_{be} - \delta_{ae}\delta_{bd}) \\
=& (C\Gamma_{tm})_{\alpha\beta}\ (C\tilde{\Gamma})_{\gamma\delta}\ \Big(\chi^{(f)}_{\substack{\alpha\\ a}}(\vec{z},t)\ \chi^{(f')}_{\substack{\beta\\ b}}(\vec{z},t)\Big)\ \Big(\bar{Q}_{\substack{\gamma\\ a}}(\vec{z},t)\ \bar{Q}_{\substack{\delta\\ b}}(\vec{z},t) - \bar{Q}_{\substack{\gamma\\ b}}(\vec{z},t)\ \bar{Q}_{\substack{\delta\\ a}}(\vec{z},t)\Big) \\
=& (C\Gamma_{tm})_{\alpha\beta}\ (C\tilde{\Gamma})_{\gamma\delta}\ \Big(\chi^{(f)}_{\substack{\alpha\\ a}}(\vec{z},t)\ \chi^{(f')}_{\substack{\beta\\ b}}(\vec{z},t)\Big)\ \Big(\bar{Q}_{\substack{\gamma\\ a}}(\vec{z},t)\ \bar{Q}_{\substack{\delta\\ b}}(\vec{z},t) + \bar{Q}_{\substack{\delta\\ a}}(\vec{z},t)\ \bar{Q}_{\substack{\gamma\\ b}}(\vec{z},t)\Big) \\
=& +2\cdot(C\Gamma_{tm})_{\alpha\beta}\ (C\tilde{\Gamma})_{\gamma\delta}\ \Big(\chi^{(f)}_{\substack{\alpha\\ a}}(\vec{z},t)\ \chi^{(f')}_{\substack{\beta\\ b}}(\vec{z},t)\Big)\ \Big(\bar{Q}_{\substack{\gamma\\ a}}(\vec{z},t)\ \bar{Q}_{\substack{\delta\\ b}}(\vec{z},t)\Big) \\
=& -2\cdot(C\Gamma_{tm})_{\alpha\beta}\ (C\tilde{\Gamma})_{\gamma\delta}\ \Big(\bar{Q}_{\substack{\gamma\\ a}}(\vec{z},t)\ \chi^{(f)}_{\substack{\alpha\\ a}}(\vec{z},t)\Big)\ \Big(\bar{Q}_{\substack{\delta\\ b}}(\vec{z},t)\ \chi^{(f')}_{\substack{\beta\\ b}}(\vec{z},t)\Big) \\
=& -2\cdot\mathcal{O}_{BB}(t)|_{r=0}
\end{aligned} \tag{3.5}$$

Here, we also used the relation $(C\tilde{\Gamma})^T = +C\tilde{\Gamma}$. The property $(C\tilde{\Gamma})^T = -C\tilde{\Gamma}$ would have led to a vanishing diquark-antidiquark operator for $r = 0$. That means, that both structures are identical for $r = 0$ (up to a constant factor). This finding will be confirmed by the numerical results in sec. 5.

3.2 Off-diagonal entries

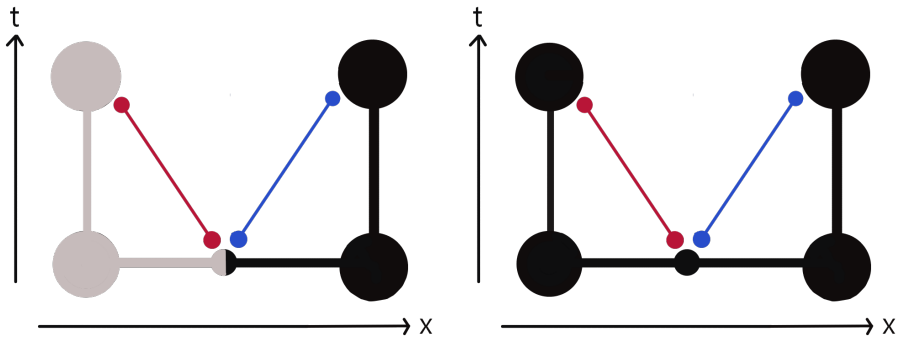

Figure 3.3: *Diagrams $C_{12}^{(1)}/C_{12}^{(4)}$ (lhs) and $C_{12}^{(2)}/C_{12}^{(3)}$ (rhs).*

In order to solve the GEVP, also the off-diagonal entries of the correlation matrix are necessary as an input, i.e. $\langle 0|\,\mathcal{O}_{BB}(t)\mathcal{O}^{\dagger}_{Dd}(0)\,|0\rangle$ and $\langle 0|\,\mathcal{O}_{Dd}(t)\mathcal{O}^{\dagger}_{BB}(0)\,|0\rangle$. Presenting the off-diagonal correlation functions is a rather technical aspect at this point and we learn nothing new in addition to the discussion of both structures in the previous section. A general remark is however, that the off-diagonal entries don't have to be real, in comparison to the diagonal entries. But due to the hermiticity of the correlation matrix one entry must be the complex conjugate of the other.

The vacuum expectation value of a created Dd state, which is annihilated as BB state reads

$$
\begin{aligned}
&\langle 0|\,\mathcal{O}_{BB}(t)\mathcal{O}^{\dagger}_{Dd}(0)\,|0\rangle \propto \qquad (3.6)\\
&-(C\Gamma^{+-}_{tw})_{\alpha\beta}\;(\gamma_0(C\Gamma^{+-}_{tw})^{\dagger}\gamma_0)_{\mu\nu}\\
&\underbrace{\langle[U(\vec{z},0;\vec{r}_1,0)_{nl}U(\vec{r}_1,0;\vec{r}_1,t)_{la}G^{(u)}(\vec{r}_1,t|\vec{z},0)\,{}^{\alpha\nu}_{an}][U(\vec{z},0;\vec{r}_2,0)_{mp}U(\vec{r}_2,0;\vec{r}_2,t)_{pb}G^{(d)}(\vec{r}_2,t|\vec{z},0)\,{}^{\beta\mu}_{bm}]\rangle}_{C^{(1)}_{12}}\\
&-(C\Gamma^{-+}_{tw})_{\alpha\beta}\;(\gamma_0(C\Gamma^{+-}_{tw})^{\dagger}\gamma_0)_{\mu\nu}\\
&\underbrace{\langle[U(\vec{z},0;\vec{r}_2,0)_{np}U(\vec{r}_2,0;\vec{r}_2,t)_{pb}G^{(u)}(\vec{r}_2,t|\vec{z},0)\,{}^{\beta\nu}_{bm}U(\vec{z},0;\vec{r}_1,0)_{ml}U(\vec{r}_1,0;\vec{r}_1,t)_{la}G^{(d)}(\vec{r}_1,t|\vec{z},0)\,{}^{\alpha\mu}_{an}]\rangle}_{C^{(2)}_{12}}\\
&+(C\Gamma^{+-}_{tw})_{\alpha\beta}\;(\gamma_0(C\Gamma^{+-}_{tw})^{\dagger}\gamma_0)_{\mu\nu}\\
&\underbrace{\langle[U(\vec{z},0;\vec{r}_1,0)_{ml}U(\vec{r}_1,0;\vec{r}_1,t)_{la}G^{(u)}(\vec{r}_1,t|\vec{z},0)\,{}^{\alpha\nu}_{an}U(\vec{z},0;\vec{r}_2,0)_{np}U(\vec{r}_2,0;\vec{r}_2,t)_{pb}G^{(d)}(\vec{r}_2,t|\vec{z},0)\,{}^{\beta\mu}_{bm}]\rangle}_{C^{(3)}_{12}}\\
&+(C\Gamma^{-+}_{tw})_{\alpha\beta}\;(\gamma_0(C\Gamma^{+-}_{tw})^{\dagger}\gamma_0)_{\mu\nu}\\
&\underbrace{\langle[U(\vec{z},0;\vec{r}_2,0)_{mp}U(\vec{r}_2,0;\vec{r}_2,t)_{pb}G^{(u)}(\vec{r}_2,t|\vec{z},0)\,{}^{\beta\nu}_{bm}][U(\vec{z},0;\vec{r}_1,0)_{nl}U(\vec{r}_1,0;\vec{r}_1,t)_{la}G^{(d)}(\vec{r}_1,t|\vec{z},0)\,{}^{\alpha\mu}_{an}]\rangle}_{C^{(4)}_{12}}
\end{aligned}
$$

The vacuum expectation value of a created BB state, which is annihilated as Dd state reads

$$
\begin{aligned}
&\langle 0|\,\mathcal{O}_{Dd}(t)\mathcal{O}^{\dagger}_{BB}(0)\,|0\rangle \propto \qquad (3.7)\\
&-(C\Gamma^{+-}_{tw})_{\alpha\beta}\;(\gamma_0(C\Gamma^{+-}_{tw})^{\dagger}\gamma_0)_{\mu\nu}\\
&\underbrace{\langle[G^{(u)}(\vec{z},t|\vec{r}_1,0)\,{}^{\alpha\nu}_{ak}U(\vec{r}_1,0;\vec{r}_1,t)_{kg}U(\vec{r}_1,t;\vec{z},t)_{ga}][G^{(d)}(\vec{z},t|\vec{r}_2,0)\,{}^{\beta\mu}_{bl}U(\vec{r}_2,0;\vec{r}_2,t)_{lf}U(\vec{r}_2,t;\vec{z},t)_{fb}]\rangle}_{C^{(1)}_{21}}\\
&-(C\Gamma^{+-}_{tw})_{\alpha\beta}\;(\gamma_0(C\Gamma^{-+}_{tw})^{\dagger}\gamma_0)_{\mu\nu}\\
&\underbrace{\langle[G^{(u)}(\vec{z},t|\vec{r}_2,0)\,{}^{\alpha\mu}_{bl}U(\vec{r}_2,0;\vec{r}_2,t)_{lf}U(\vec{r}_2,t;\vec{z},t)_{fa}G^{(d)}(\vec{z},t|\vec{r}_1,0)\,{}^{\beta\nu}_{ak}U(\vec{r}_1,0;\vec{r}_1,t)_{kg}U(\vec{r}_1,t;\vec{z},t)_{gb}]\rangle}_{C^{(2)}_{21}}\\
&+(C\Gamma^{+-}_{tw})_{\alpha\beta}\;(\gamma_0(C\Gamma^{+-}_{tw})^{\dagger}\gamma_0)_{\mu\nu}\\
&\underbrace{\langle[G^{(u)}(\vec{z},t|\vec{r}_1,0)\,{}^{\alpha\nu}_{ak}U(\vec{r}_1,0;\vec{r}_1,t)_{kg}U(\vec{r}_1,t;\vec{z},t)_{gb}G^{(d)}(\vec{z},t|\vec{r}_2,0)\,{}^{\beta\mu}_{bl}U(\vec{r}_2,0;\vec{r}_2,t)_{lf}U(\vec{r}_2,t;\vec{z},t)_{fa}]\rangle}_{C^{(3)}_{21}}\\
&+(C\Gamma^{+-}_{tw})_{\alpha\beta}\;(\gamma_0(C\Gamma^{-+}_{tw})^{\dagger}\gamma_0)_{\mu\nu}\\
&\underbrace{\langle[G^{(u)}(\vec{z},t|\vec{r}_2,0)\,{}^{\alpha\mu}_{bl}U(\vec{r}_2,0;\vec{r}_2,t)_{lf}U(\vec{r}_2,t;\vec{z},t)_{fb}][G^{(d)}(\vec{z},t|\vec{r}_1,0)\,{}^{\beta\nu}_{ak}U(\vec{r}_1,0;\vec{r}_1,t)_{kg}U(\vec{r}_1,t;\vec{z},t)_{ga}]]\rangle}_{C^{(4)}_{21}}
\end{aligned}
$$

Both correlation functions have the same proportionality factor, which is $2K$. The corresponding diagrammatic representations are shown in fig. 3.3 and fig. 3.4.

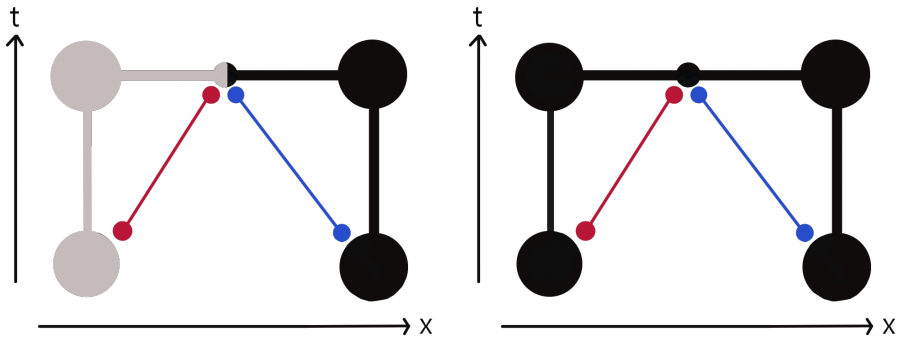

Figure 3.4: *Diagrams $C_{21}^{(1)}/C_{21}^{(4)}$ (lhs) and $C_{21}^{(2)}/C_{21}^{(3)}$ (rhs).*

Calculating the correlation functions, shown in eq. 3.2, 3.4, 3.6 and 3.7 for different varying heavy quark separations r and for the choices $\Gamma = (1+\gamma_0)\gamma_5$ and $\tilde{\Gamma} = (1+\gamma_0)\gamma_j$, $j = 1, 2, 3$ is now the main task. It is stressed at this point, that the different operators describe different structures, but still carry the same quantum numbers. The technical realization is addressed in the next section.

4 Numerical implementation

In the following, it is explained how the computation of the previously discussed correlation functions is technically realized. After having discussed the different gauge ensembles together with their parameters used to solve the path integral over the gauge field, we discuss the use smearing techniques to improve the signal-to-noise ratio in our calculations. Then, it is shown how the light quark propagators are estimated using stochastic timeslice sources and finally, we discuss symmetries of the twisted basis propagator and how we can profit from them.

4.1 Lattice ensembles

In this work, the lattice computations are performed using three ensembles of gauge link configurations with two degenerate dynamical quark flavours, generated by the European Twisted Mass Collaboration (ETMC) [23]. The quark action is Wilson twisted mass tuned to maximal twist, c.f. sec. 2.4, while the gluon action is tree-level Symanzik improved. Thus, the computed spectral quantities, i.e. the lattice potentials, are $\mathcal{O}(a)$ improved. The parameters of these ensembles are collected in tab. 4.1. Shown are the inverse bare coupling β, lattice spacing a, lattice size $(L/a)^3 \times T/a$, bare twisted light sea quark mass in lattice units $a\mu$, pion mass m_π and the number of used gauge configurations. We profit from the

Ensemble	β	a in fm	$(L/a)^3 \times T/a$	$a\mu$	m_π [MeV]	# gauges
B40.24	3.90	0.079(3)	$24^3 \times 48$	0.004	340	108
C30.32	4.05	0.063(2)	$32^3 \times 64$	0.003	325	98
D20.24	4.20	0.0514(8)	$24^3 \times 48$	0.002	284	211

Table 4.1: *Parameters of $N_f = 2$ gauge ensembles gererated by the ETMC.*

fact, that all gauge ensembles have different lattice spacings. This will enable us to analyze the lattice potentials and eigenvectors, resulting from the GEVP for many different heavy quark separations. Afterwards we can summarize all results in one diagramm to obtain a fine resolution of these quantities. To this end, the differing properties of the ensembles, e.g. (slightly) different pion masses and lattice sizes are ignored.

4.2 Smearing techniques

Ground state energies are extracted from the effective mass plateau for large euclidean times, where the signal-to-noise ratio is getting worse. Smearing techniques are used to increase the overlap of trial states with low lying energy eigenstates. That in turn means at the same time, that excited state are better suppressed. Consequently, the ground state plateau shifts to smaller temporal separations, where the signal-to-noise ratio is acceptable.

APE smearing of spatial links

Performing the average over neighboring spatial loops of link variables improves the overlap. After N_{APE} iterations APE smeared spatial links are given by [24]

$$U^{(N_{\mathrm{APE}})}(x, x+e_k) = P_{\mathrm{SU(3)}}\Bigg(U^{(N_{\mathrm{APE}}-1)}(x, x+e_k) + \alpha_{\mathrm{APE}} \sum_{j=\pm1,\pm2,\pm3}^{j\neq\pm k} U^{(N_{\mathrm{APE}}-1)}(x, x+e_j)$$
$$U^{(N_{\mathrm{APE}}-1)}(x+e_j, x+e_j+e_k) U^{(N_{\mathrm{APE}}-1)}(x+e_j+e_k, x+e_k)\Bigg),$$

where $U^{(0)}$ denote the original unsmeared links. α_{APE} is a weighting parameter and $P_{SU(3)}$ denotes projection back to $SU(3)$.

Gaussian smearing of light quark operators

After N_{Gauss} iterations Gaussian smeared light quark quark operators are given by [25, 26]

$$\chi^{(N_{\mathrm{Gauss}})}(x) =$$
$$= \frac{1}{1+6\kappa}\Bigg(\chi^{(N_{\mathrm{Gauss}}-1)}(x) + \kappa_{\mathrm{Gauss}} \sum_{j=\pm1,\pm2,\pm3} U^{(N_{\mathrm{APE}})}(x, x+e_j)\chi^{(N_{\mathrm{Gauss}}-1)}(x+e_j)\Bigg),$$

where $\chi^{(0)}$ are the original unsmeared light quark operators and $U^{(N_{APE})}$ denote APE smeared spatial links. The parameter κ_{Gauss} has to be adjusted.

HYP2 - Smearing

In static-light correlation functions, HYP2 smearing helps to improve the signal to noise ratio by reducing the self energy of the static quark. For each line of temporal links the HYP smearing algorithm performs smearing over all loops of links inside a hypercube of a certain width. Details of the smearing process depend on three parameters α_1, α_2 and α_3. For a more detailed discussion about HYP2 smearing and its use in static actions, see Refs. [27, 28, 18, 19].

All computations were performed with the same choice for the smearing parameters.

- APE Smearing: $N_{APE} = 30$ and $\alpha_{APE} = 0.5$.
- Gaussian Smearing: $N_{Gauss} = 50$ and $\kappa_{Gauss} = 0.5$
- HYP2 Smearing: $\alpha_1 = \alpha_2 = 1$, $\alpha_3 = 0.5$

4.3 Stochastic timeslice-to-all propagators

Several efficient techniques for the numerical expensive computation of light quark propagators are presented in [29]. Here, only the timeslice source method is briefly discussed.

Using this technique, we can stochastically estimate propagators from any space point $\vec{y}$ in a given time-slice t_0 to any other spacetime point $(\vec{x}, t)$. To this end, linear systems have to

be solved, labeled by $n = 1, \ldots, N_S$.

$$\sum_y D^{(f)}(x|y)\,{}^{\alpha\beta}_{ab}\,\phi^{(f)}(y)\,{}^{\beta}_{b}[t_0,n] = \xi(x)\,{}^{\alpha}_{a}[t_0,n] \quad , \quad \xi(x)\,{}^{\alpha}_{a}[t_0,n] = \delta(x_0,t_0)\Xi(\mathbf{x})\,{}^{\alpha}_{a}[n], \tag{4.1}$$

where $D^{(f)}(x|y)\,{}^{\alpha\beta}_{ab}$ denotes for example the twisted mass Dirac operator for either the up- or the down quark. With the following choice for the stochastic sources (both "$\pm$" signs are chosen randomly and independently of one another)

$$\xi(x)\,{}^{\alpha}_{a}[t_0,n] = \delta(x_0,t_0)\Big(\pm\frac{1}{\sqrt{2}} \pm i\frac{1}{\sqrt{2}}\Big)$$

we work with random numbers $\Xi\,{}^{\alpha}_{a}(\mathbf{x})[n]$ satisfying

$$\frac{1}{N}\sum_{n=1}^{N}\Xi^{*}\,{}^{\alpha}_{a}(\mathbf{x})[n]\Xi\,{}^{\beta}_{b}(\mathbf{y})[n] = \delta_{ab}\delta_{\alpha\beta}\delta(\mathbf{x};\mathbf{y}) + \mathrm{O}\Big(\frac{1}{\sqrt{N}}\Big) \text{ off-diagonal noise.} \tag{4.2}$$

Using 4.1 and 4.2 it is straightforward to show

$$G^{(f)}(y;\mathbf{x},t_0) \;=\; \frac{1}{N}\sum_{n=1}^{N}\phi^{(f)}(y)[t_0,n]\xi(\mathbf{x},t_0)[t_0,n]^{\dagger} + \mathrm{O}\Big(\frac{1}{\sqrt{N}}\Big) \text{ off-diagonal noise.} \tag{4.3}$$

Stochastic timeslice-to-all propagators are very flexible and allow to exploit translational invariance. Correlation functions can be evaluated at a large number of source points, while only a few inversions have to be performed. Due to the larger lattice volume of the "$C30.32$" ensemble, it is justified to consider less gauge field configurations for the numerical computations compared to the other two ensembles. Here, we can evaluate the correlation functions with 32^3 samples (per configuration) instead of 24^3.

A disadvantage of this technique is, that additional stochastic noise is introduced and it may be, that the signal gets lost in the noise if these techniques are applied naively. In my calculations, we found an acceptable signal-to-noise ratio using $N_S = 12$ inversions for the light quark propagator. Another strategy to improve the signal besides increasing the number of sources is to perform the inversions for multiple different timeslices. After having computed the correlation functions with the propagators, starting from different timeslices, one can then average over the results.

Analogue to eq. 4.3, the product of two light quark propagators, which occurs in our correlation functions, can be written as

$$G_q^{(f)}(\vec{x}_1,t_1|\vec{y}_1,t_0)\,{}^{\alpha\beta}_{ab}\;G_q^{(f')}(\vec{x}_2,t_2|\vec{y}_2,t_0)\,{}^{\gamma\delta}_{cd} = \frac{1}{N(N-1)}\sum_{n\neq m}^{N}\Phi^{(f)}\,{}^{\alpha}_{a}(\vec{x}_1,t_1)[n,t_0]\;\xi^{\dagger}\,{}^{\beta}_{b}(\vec{y}_1,t_0)[n,t_0]$$
$$\Phi^{(f')}\,{}^{\gamma}_{c}(\vec{x}_2,t_2)[m,t_0]\;\xi^{\dagger}\,{}^{\delta}_{d}(\vec{y}_2,t_0)[m,t_0]$$

Note that each propagator needs to be estimated by a different pair of stochastic sources $\xi[n]$ and corresponding inversions $\phi[n]$ (guaranteed here by $\sum_{n\neq\tilde{n}}$).

In the following, the mesonic molecule correlation function, c.f. eq. 3.2, is used as an example, to show explicitly how the correlation functions are computed in the contraction codes by means of the stochastic quark propagators. A constant prefactor for the correlation function is omitted to improve the readability and thus, we write "$\propto$" instead of "$=$".

$$
\begin{aligned}
&\langle 0|\, \mathcal{O}_{BB}(t)\mathcal{O}^{\dagger}_{BB}(0)\,|0\rangle\,|_{I=0} \propto \\
&+ \sum_{n\neq m}^{N} \langle\; U(\vec{r}_1,0;\vec{r}_1,t)_{ca}\; \Phi^{(u)}_{\substack{\alpha\\ a}}(\vec{r}_1,t)[n,0]\; (C\Gamma^{+-}_{tw})_{\alpha\beta}\; U(\vec{r}_2,0;\vec{r}_2,t)_{db}\; \Phi^{(d)}_{\substack{\beta\\ b}}(\vec{r}_2,t)[m,0] \\
&\xi^{\dagger}_{\substack{\lambda\\ d}}(\vec{r}_2,0)[m,0]\; (\gamma_0(C\Gamma^{+-}_{tw})^{\dagger}\gamma_0)_{\lambda\kappa}\; \xi^{\dagger}_{\substack{\kappa\\ c}}(\vec{r}_1,0)[n,0]\;\rangle \\
&+ \sum_{n\neq m}^{N} \langle\; U(\vec{r}_1,0;\vec{r}_1,t)_{ca}\; \Phi^{(u)}_{\substack{\alpha\\ a}}(\vec{r}_1,t)[n,0]\; (C\Gamma^{+-}_{tw})_{\alpha\beta}\; U(\vec{r}_2,0;\vec{r}_2,t)_{db}\; \Phi^{(d)}_{\substack{\beta\\ b}}(\vec{r}_2,t)[m,0] \\
&\xi^{\dagger}_{\substack{\lambda\\ d}}(\vec{r}_2,0)[n,0]\; (\gamma_0(C\Gamma^{-+}_{tw})^{\dagger}\gamma_0)_{\lambda\kappa}\; \xi^{\dagger}_{\substack{\kappa\\ c}}(\vec{r}_1,0)[m,0]\;\rangle \\
&+ \sum_{n\neq m}^{N} \langle\; U(\vec{r}_1,0;\vec{r}_1,t)_{ca}\; \Phi^{(d)}_{\substack{\alpha\\ a}}(\vec{r}_1,t)[m,0]\; (C\Gamma^{-+}_{tw})_{\alpha\beta}\; U(\vec{r}_2,0;\vec{r}_2,t)_{db}\; \Phi^{(u)}_{\substack{\beta\\ b}}(\vec{r}_2,t)[n,0] \\
&\xi^{\dagger}_{\substack{\lambda\\ d}}(\vec{r}_2,0)[m,0]\; (\gamma_0(C\Gamma^{+-}_{tw})^{\dagger}\gamma_0)_{\lambda\kappa}\; \xi^{\dagger}_{\substack{\kappa\\ c}}(\vec{r}_1,0)[n,0]\;\rangle \\
&+ \sum_{n\neq m}^{N} \langle\; U(\vec{r}_1,0;\vec{r}_1,t)_{ca}\; \Phi^{(d)}_{\substack{\alpha\\ a}}(\vec{r}_1,t)[m,0]\; (C\Gamma^{-+}_{tw})_{\alpha\beta}\; U(\vec{r}_2,0;\vec{r}_2,t)_{db}\; \Phi^{(u)}_{\substack{\beta\\ b}}(\vec{r}_2,t)[n,0] \\
&\xi^{\dagger}_{\substack{\lambda\\ d}}(\vec{r}_2,0)[n,0]\; (\gamma_0(C\Gamma^{-+}_{tw})^{\dagger}\gamma_0)_{\lambda\kappa}\; \xi^{\dagger}_{\substack{\kappa\\ c}}(\vec{r}_1,0)[m,0]\;\rangle
\end{aligned}
$$

In each of the four diagrams, the inversions Φ combine with the products of links U, coming from the heavy quark propagators and the spin matrix $C\Gamma$ to a matrix in colour space. This matrix is multiplied with another colour matrix, resulting from the combination of the sources with $\gamma_0\Gamma^{\dagger}C^{\dagger}\gamma_0$. Finally the correlation function is evaluated as trace over remaining colour matrix.

4.4 Symmetries of the twisted basis propagator

Applying symmetries of the (twisted basis) propagator to the correlation functions leads to relations between individual diagrams, which can be checked in the numerical results to support their credibility. Furthermore, averaging over related diagrams helps to improve the statistical precision. The following four symmetries are considered in this thesis.

γ_5 Hermiticity

$$G(x,y) = \tau_1\gamma_5\Big(G(y,x)\Big)^{\dagger}\gamma_5\tau_1$$

Parity

$$G(\vec{x},\vec{y}) = \tau_1\gamma_0 G(-\vec{x},-\vec{y})\gamma_0\tau_1$$

$$\begin{aligned} U_0(t,\vec{x}) &\xrightarrow{\mathcal{P}} U_0(t,\vec{x})^{\mathcal{P}} = U_0(t,-\vec{x}) \\ U_i(t,\vec{x}) &\xrightarrow{\mathcal{P}} U_i(t,\vec{x})^{\mathcal{P}} = U_i(t,-\vec{x}-\hat{i})^\dagger \end{aligned}$$

Time reversal

$$G(t_1,t_2) = \tau_1\gamma_0\gamma_5 G(-t_1,-t_2)\gamma_5\gamma_0\tau_1$$

$$\begin{aligned} U_0(t,\vec{x}) &\xrightarrow{\mathcal{T}} U_0(t,\vec{x})^{\mathcal{T}} = U_0(-t-1,\vec{x})^\dagger \\ U_i(t,\vec{x}) &\xrightarrow{\mathcal{T}} U_i(t,\vec{x})^{\mathcal{T}} = U_i(-t,\vec{x}) \end{aligned}$$

Charge conjugation

$$G(x,y) = \gamma_0\gamma_2\Big(G(y,x)\Big)^T\gamma_2\gamma_0$$

$$U_\mu(t,\vec{x}) \xrightarrow{\mathcal{C}} U_\mu(t,\vec{x})^{\mathcal{C}} = U_\mu(t,\vec{x})^* = (U_\mu(t,\vec{x})^\dagger)^T$$

In the above shown symmetries, τ_1 denotes the first Pauli matrix, acting in flavour space. It is responsible for the exchange of the quark flavours u and d when the symmetries are applied to correlation functions. The gamma matrices act in spin space of course and the propagators both in spin- and colour space. Every computed correlation function has been checked for the four presented symmetries and averaging over related diagrams was performed afterwards. In the following, an example for relating two diagrams via symmetries is shown.

Example

The first diagram of the mesonic molecule correlation function, i.e. $C_{11}^{(1)}$ reads (without prefactors)

$$(C\Gamma_{tw}^{+-})_{\alpha\beta}(\gamma_0(C\Gamma_{tw}^{+-})^\dagger\gamma_0)_{\lambda\kappa}\ \langle[U(\vec{r}_1,0;\vec{r}_1,t)_{ca}\ G^{(u)}(\vec{r}_1,t|\vec{r}_1,0)_{\substack{\alpha\kappa\\ac}}][U(\vec{r}_2,0;\vec{r}_2,t)_{db}\ G^{(d)}(\vec{r}_2,t|\vec{r}_2,0)_{\substack{\beta\lambda\\bd}}]\rangle$$

In the following, the γ_5 hermiticity is used for the twisted mass propagators with the choice $\Gamma_{tw}^{+-} = \gamma_5$.

$$\begin{aligned} \longrightarrow\ & (\gamma_5 C\Gamma_{tw}^{+-}\gamma_5)_{\alpha\beta}(\gamma_5\gamma_0(C\Gamma_{tw}^{+-})^\dagger\gamma_0\gamma_5)_{\lambda\kappa} \\ & \langle[U(\vec{r}_1,0;\vec{r}_1,t)_{ca}\ \Big(G^{(d)}(\vec{r}_1,0|\vec{r}_1,t)\Big)^\dagger_{\substack{\alpha\kappa\\ac}}][U(\vec{r}_2,0;\vec{r}_2,t)_{db}\ \Big(G^{(u)}(\vec{r}_2,0|\vec{r}_2,t)\Big)^\dagger_{\substack{\beta\lambda\\bd}}]\rangle \\ \longrightarrow\ & (C\Gamma_{tw}^{+-})^*_{\alpha\beta}(\gamma_0(C\Gamma_{tw}^{+-})^\dagger\gamma_0)^*_{\lambda\kappa} \\ & \langle[U(\vec{r}_1,t;\vec{r}_1,0)^*_{ac}\ \Big(G^{(d)}(\vec{r}_1,0|\vec{r}_1,t)\Big)^*_{\substack{\kappa\alpha\\ca}}][U(\vec{r}_2,t;\vec{r}_2,0)^*_{bd}\ \Big(G^{(u)}(\vec{r}_2,0|\vec{r}_2,t)\Big)^*_{\substack{\beta\lambda\\db}}]\rangle \\ \longrightarrow\ & (C\Gamma_{tw}^{+-})^*_{\alpha\beta}(\gamma_0(C\Gamma_{tw}^{+-})^\dagger\gamma_0)^*_{\lambda\kappa} \\ & \langle[U(\vec{r}_1,0;\vec{r}_1,-t)^*_{ac}\ \Big(G^{(d)}(\vec{r}_1,-t|\vec{r}_1,0)\Big)^*_{\substack{\alpha\kappa\\ca}}][U(\vec{r}_2,0;\vec{r}_2,-t)^*_{bd}\ \Big(G^{(u)}(\vec{r}_2,-t|\vec{r}_2,0)\Big)^*_{\substack{\beta\lambda\\db}}]\rangle \end{aligned}$$

We have found, that the first and fourth diagram in the mesonic molecule correlation function are related via

$$C_{11}^{(1)}(+t) = \left(C_{11}^{(4)}(-t)\right)^*$$

In this calculation it was used, that

$$\begin{aligned}(\gamma_5 C\Gamma_{tw}^{+-}\gamma_5) &= +(C\Gamma_{tw}^{+-})\\ (\gamma_5\gamma_0(C\Gamma_{tw}^{+-})^\dagger\gamma_0\gamma_5) &= +(\gamma_0(C\Gamma_{tw}^{+-})^\dagger\gamma_0)\end{aligned}$$

for $\Gamma_{tw}^{+-} = \gamma_5$. The signs on the right hand side could also be "$-$" for other choices.

Moreover, we have used

$$U(\vec{x},t_1;\vec{x},t_2)_{ab} = U(\vec{x},t_2;\vec{x},t_1)^\dagger_{ab} = U(\vec{x},t_2;\vec{x},t_1)^*_{ba}$$

This equation means that the conjugate transpose reverses the direction of the links and consequently taking the complex conjugate and reversing the direction by hand changes nothing.

Finally, relabeling of indices ($\alpha \leftrightarrow \kappa$, $\beta \leftrightarrow \lambda$), using eq. A.1 and the fact that, we are allowed to shift all times by the same value (because the correlation function only depends on time differences) lead to the final result.

Several checks of the symmetries of the computed numerical results are shown in sec. 5.1. Moreover, in sec. A.4, tables can be found, which give a complete overview over all applied symmetries in this work. In the following, the BB correlation function is used as an example, to explain the labeling in these tables, which is necessary to understand them. For the choice $\Gamma = (1+\gamma_0)\gamma_5$ (pb), the (light quark) spin structure reads (c.f. eq. 3.2)

$$\begin{aligned}
&\underbrace{(C\Gamma_{tm}^{+-})_{\alpha\beta}\ (\gamma_0(C\Gamma_{tm}^{+-})^\dagger\gamma_0)_{\mu\nu}}_{C_{11}^{(1)}} + \underbrace{(C\Gamma_{tm}^{+-})_{\alpha\beta}\ (\gamma_0(C\Gamma_{tm}^{-+})^\dagger\gamma_0)_{\mu\nu}}_{C_{11}^{(2)}} \\
&\underbrace{(C\Gamma_{tm}^{-+})_{\alpha\beta}\ (\gamma_0(C\Gamma_{tm}^{+-})^\dagger\gamma_0)_{\mu\nu}}_{C_{11}^{(3)}} + \underbrace{(C\Gamma_{tm}^{-+})_{\alpha\beta}\ (\gamma_0(C\Gamma_{tm}^{-+})^\dagger\gamma_0)_{\mu\nu}}_{C_{11}^{(4)}} \\
= &- \underbrace{(\gamma_0\gamma_2\gamma_5)_{\alpha\beta}(\gamma_0\gamma_2\gamma_5)^{(1)}_{\mu\nu}}_{C_1} - i\underbrace{(\gamma_0\gamma_2\gamma_5)_{\alpha\beta}(\gamma_2)^{(1)}_{\mu\nu}}_{C_5} + i\underbrace{(\gamma_2)_{\alpha\beta}(\gamma_0\gamma_2\gamma_5)^{(1)}_{\mu\nu}}_{C_9} - \underbrace{(\gamma_2)_{\alpha\beta}(\gamma_2)^{(1)}_{\mu\nu}}_{C_{13}} \\
&- \underbrace{(\gamma_0\gamma_2\gamma_5)_{\alpha\beta}(\gamma_0\gamma_2\gamma_5)^{(2)}_{\mu\nu}}_{C_2} + i\underbrace{(\gamma_0\gamma_2\gamma_5)_{\alpha\beta}(\gamma_2)^{(2)}_{\mu\nu}}_{C_6} + i\underbrace{(\gamma_2)_{\alpha\beta}(\gamma_0\gamma_2\gamma_5)^{(2)}_{\mu\nu}}_{C_{10}} + \underbrace{(\gamma_2)_{\alpha\beta}(\gamma_2)^{(2)}_{\mu\nu}}_{C_{14}} \\
&- \underbrace{(\gamma_0\gamma_2\gamma_5)_{\alpha\beta}(\gamma_0\gamma_2\gamma_5)^{(3)}_{\mu\nu}}_{C_3} - i\underbrace{(\gamma_0\gamma_2\gamma_5)_{\alpha\beta}(\gamma_2)^{(3)}_{\mu\nu}}_{C_7} - i\underbrace{(\gamma_2)_{\alpha\beta}(\gamma_0\gamma_2\gamma_5)^{(3)}_{\mu\nu}}_{C_{11}} + \underbrace{(\gamma_2)_{\alpha\beta}(\gamma_2)^{(3)}_{\mu\nu}}_{C_{15}} \\
&- \underbrace{(\gamma_0\gamma_2\gamma_5)_{\alpha\beta}(\gamma_0\gamma_2\gamma_5)^{(4)}_{\mu\nu}}_{C_4} + i\underbrace{(\gamma_0\gamma_2\gamma_5)_{\alpha\beta}(\gamma_2)^{(4)}_{\mu\nu}}_{C_8} - i\underbrace{(\gamma_2)_{\alpha\beta}(\gamma_0\gamma_2\gamma_5)^{(4)}_{\mu\nu}}_{C_{12}} - \underbrace{(\gamma_2)_{\alpha\beta}(\gamma_2)^{(4)}_{\mu\nu}}_{C_{16}}
\end{aligned} \tag{4.4}$$

We benefit from multiplying out the spin matrices, which leads to the subdivision of each diagram into four correlators. First, it is easier to relate correlators via the above shown

symmetries than relating whole diagrams. Second, we can combine the correlators also to other Γ structures, i.e. we are more flexible in this case. While considering all correlators C_1 - C_{16} corresponds to $\Gamma = (1 + \gamma_0)\gamma_5$ (by construction), considering only C_1 - C_4 corresponds to $\Gamma = \gamma_5$ and considering only C_{13} - C_{16} to $\Gamma = \gamma_0\gamma_5$. We use this notation also in the tables for the symmetries of the other computed correlation functions.

5 Numerical results

In this section, the numerical results are presented and discussed. First, we check correlators for their symmetries. Afterwards, the elements of the 2×2 correlation matrix are shown and an orthogonality relation for its states is computed. Then, we use 1×1 correlation matrices, to compute effective masses for the BB and Dd operators and extract the corresponding potentials for both cases by fitting the ground state plateaus. Finally, the main result of this thesis is the investigation of the internal tetraquark structure via eigenvectors, resulting from the solution of the GEVP, for a large range of heavy quark separations.

For the analysis in sec. 5.1 - 5.4, it is sufficient to discuss the quantities only for the "B40.24" ensemble as an example. In sec. 5.5 - 5.6 all three ensembles are considered in the results.

5.1 Symmetry checks

In fig. 5.1, four different correlators of the BB correlation function are shown together with their related counterparts (c.f. tab. A.4).

The first two diagrams in fig. 5.1 are related via the time reversal symmetry $\mathcal{T}$ according to

$$C_2(+t) = +C_3(-t)$$

and the next two diagrams via the γ_5-Hermiticity.

$$C_5(+t) = +C_{12}^*(-t)$$

The charge conjugation symmetry $\mathcal{C}$ relates the next two correlators

$$C_{16}(+t) = +C_{16}(-t)$$

and finally, the two diagrams at bottom are related via the parity symmetry $\mathcal{P}$.

$$C_{10}(+t) = -C_{11}(+t)$$

Of course, the here shown relations are only examples. After having performed the lattice simulations, all symmetries were checked and applied for all entries of the correlation matrix. We have 4 symmetries for each of the 4 matrix entries. Each entry consists of 4 diagrams and they are in turn composed of 4 correlators. That means that 256 symmetry relations were applied in total.

It is absolutely necessary to observe that the correlators C_5 - C_{12} are purely imaginary, because according to eq. 4.4, these correlators have to be multiplied by "i" in the next step. In this way, the BB correlation function becomes a purely real quantity.

5.2 Entries of the correlation matrix

Fig. 5.2 shows the entries of the 2×2 correlation matrix, defined in eq. 3.1. Before the computed correlation functions enter the GEVP, the correlation functions in it are normalized in the following way.

$$C_{ij} \quad \longrightarrow \quad \begin{pmatrix} \frac{C_{11}}{\sqrt{C_{11}(t=1)C_{11}(t=1)}} & \frac{C_{12}}{\sqrt{C_{11}(t=1)C_{22}(t=1)}} \\ \frac{C_{21}}{\sqrt{C_{22}(t=1)C_{11}(t=1)}} & \frac{C_{22}}{\sqrt{C_{22}(t=1)C_{22}(t=1)}} \end{pmatrix}$$

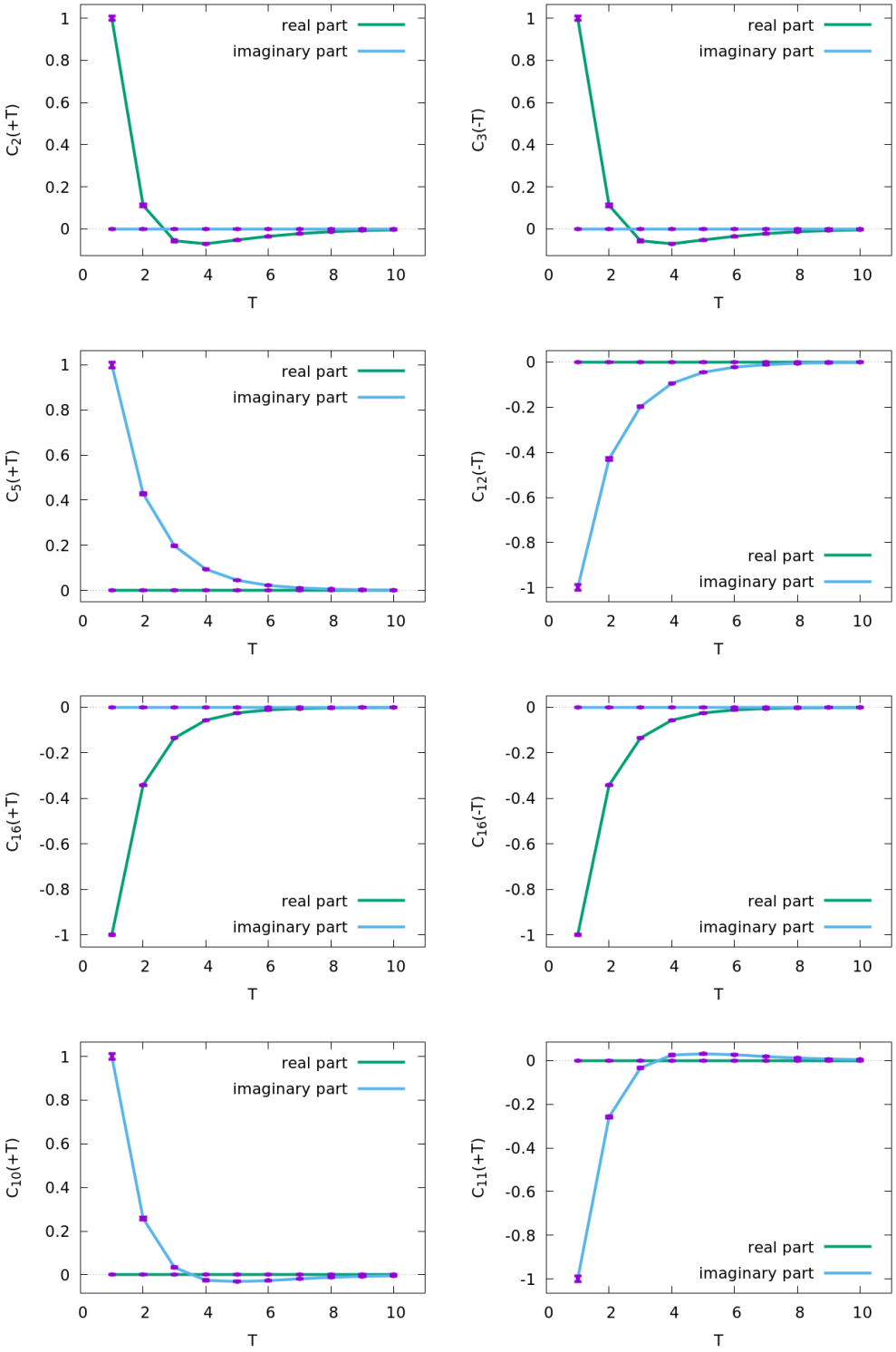

Figure 5.1: *Symmetry checking of BB correlators. Diagrams on the left are related to those on the right. The shown correlators were computed for heavy quark separation $r = 0$ using the "B40.24" ensemble.*

This explains why all diagonal entries are equal to one for euclidean time $t = 1$.

We observe, that also the off-diagonal entries are real. This has the consequence, that they have to be identical to each other because the correlation matrix is hermitian by definition. Indeed, after computing both off-diagonal entries using individual contraction codes, it turns out that this is the case. Also symmetry averaging helps in this context, because it relates both off-diagonal entries with each other, c.f. tab. A.6 and tab. A.7. This removes differences due to statistical fluctuations.

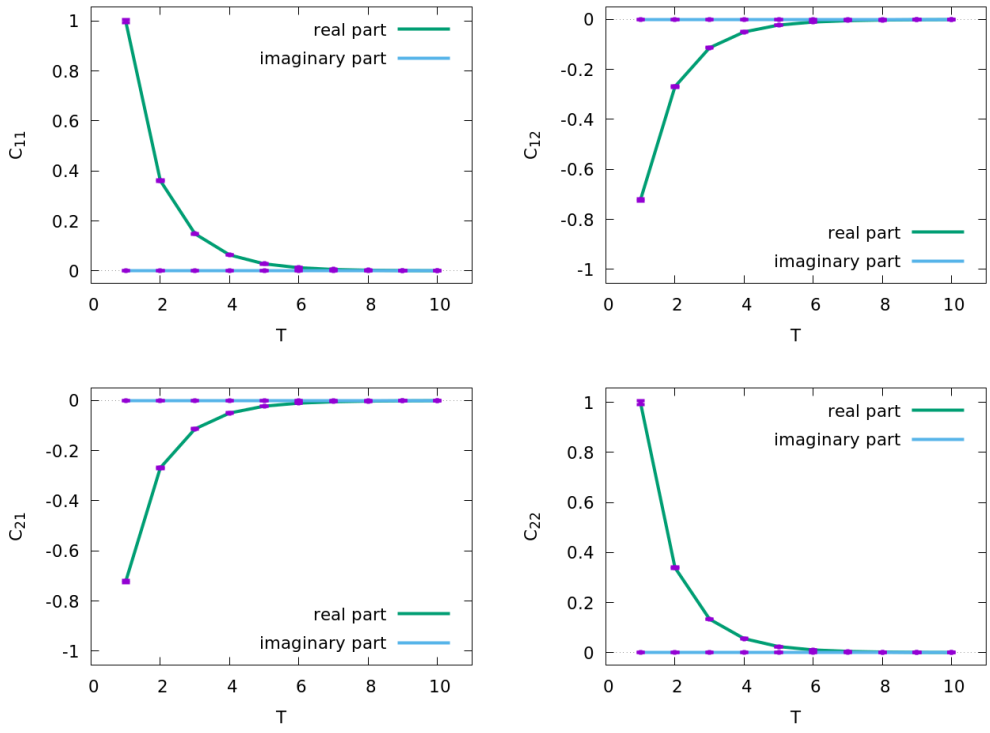

Figure 5.2: *Entries of the* 2×2 *correlation matrix for heavy quark separation* $r = 5$ *and for* $\Gamma_{BB} = (1+\gamma_0)\gamma_5$, $\Gamma_{Dd} = (1+\gamma_0)\gamma_5$. *The "B40.24" ensemble was used for the computation of the shown results.*

At least for the case $r = 0$, this property of the correlation matrix could have been predicted, because we found out, that both operators are identical up tp a negative constant factor in this limit, c.f. eq. 3.5.

$$\langle \mathcal{O}_{BB} \mathcal{O}^{\dagger}_{Dd} \rangle \propto - \underbrace{\langle \mathcal{O}_{BB} \mathcal{O}^{\dagger}_{BB} \rangle}_{>0}$$

Consequently, all four entries in the matrix are exactly the same (up to a relative sign between diagonal- and off-diagonal elements) for $r = 0$. For increasing heavy quark separations, the off-diagonal entries become smaller and smaller compared to the diagonal entries. This behavior is analyzed quantitatively in the next section.

5.3 Orthogonality relation

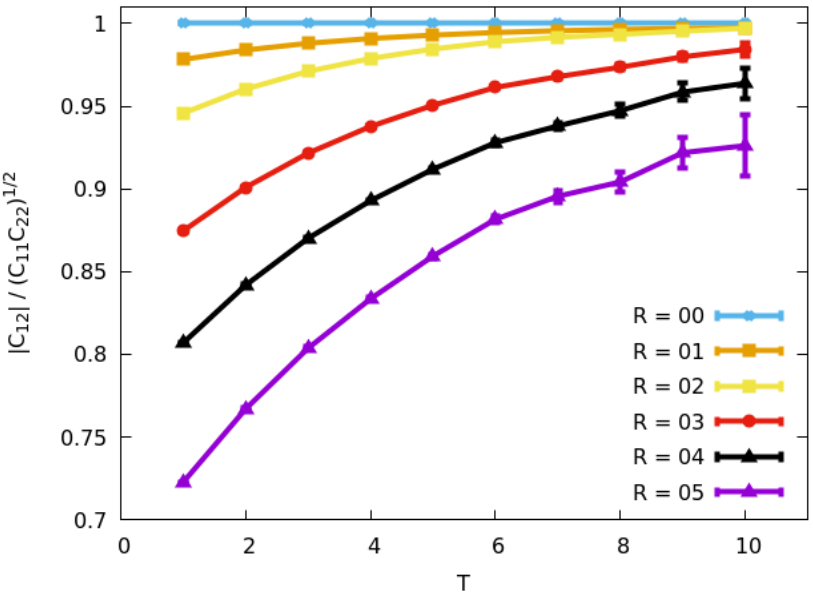

Figure 5.3: *The orthogonality of the BB / Dd structures is investigated for different heavy quark separations and for* $\Gamma_{BB} = (1+\gamma_0)\gamma_5$, $\Gamma_{Dd} = (1+\gamma_0)\gamma_5$ *using the "B40.24" ensemble.*

The following orthogonality relation

$$\frac{|C_{12}(t)|}{\sqrt{C_{11}(t)C_{22}(t)}}$$

tells us, whether the two states in the correlation matrix are orthogonal, if it yields zero or equal to each other if it is one. Of course, everything between is also possible.

In fig. 5.3, this relation is shown in order to estimate the orthogonality of the BB and Dd structures. It is shown for a large range of euclidean times for several fixed heavy quark separations. It is not surprising, that both operators are identical in the limit $r \to 0$. We knew about this property since the discussion in sec. 3.1. It is however a good idea, to check whether the computed correlation functions confirm this relation, because affirming this prediction using results form individual and independent contraction codes helps to support the credibility of the numerical results.

Of course, the mesonic molecule and the diquark-antidiquark operators differ more and more for growing heavy quark separations, due to their different colour structure. While separating the heavy quarks means to separate two B mesons for the mesonic molecule, it means to further extend the static antidiquark in the diquark-antidiquark picture.

The growing error bars for larger heavy quark separations result from a worse signal-to-noise ratio for the correlation functions in this region, especially for the diquark-antidiquark correlation function C_{22}. Fig. 5.4 shows the signal-to-noise ratios in the correlation matrix for heavy quark separation $r = 5$. The best signal can be found for the mesonic molecule

correlation function. Considering the diquark-antidiquark operator either as creation- or annihilation operator in one of the off-diagonal entries leads to a slightly worse signal. The diquark-antidiquark correlation function has the worst signal-to-noise ratio.

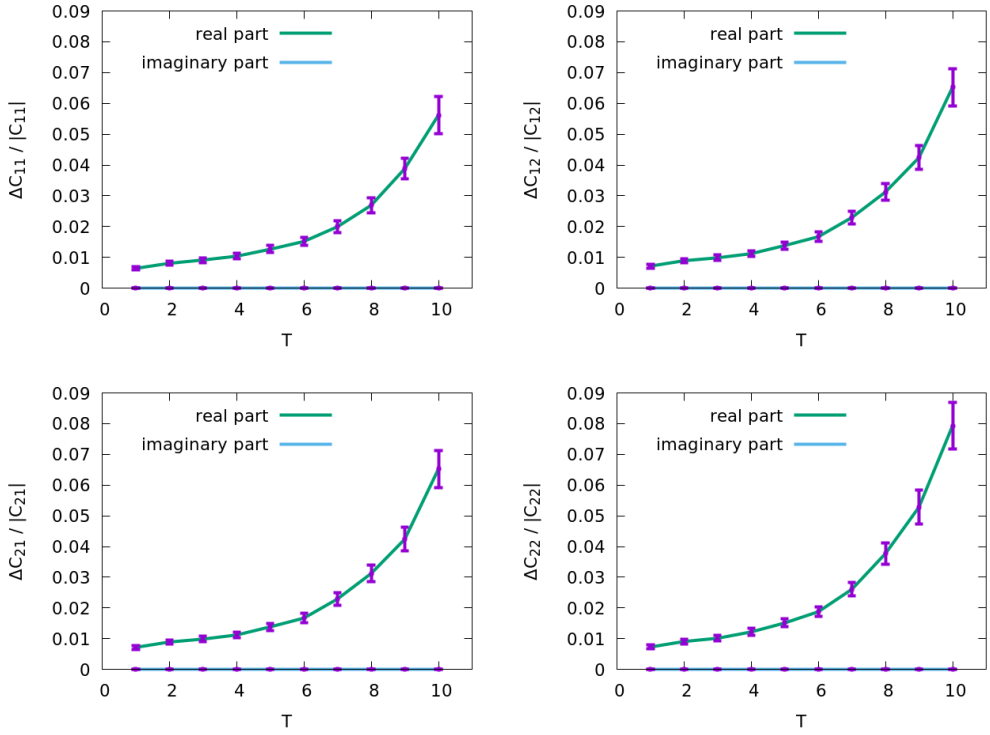

Figure 5.4: *Signal-to-noise ratios for the entries of the* 2×2 *correlation matrix for* $r = 5$ *and with* $\Gamma_{BB} = (1 + \gamma_0)\gamma_5$, $\Gamma_{Dd} = (1 + \gamma_0)\gamma_5$. *The "B40.24" ensemble was used for the computation of the shown results.*

5.4 Effective mass plateaus

In this section, several effective masses are shown, resulting from the solution of the GEVP with 1×1 matrices, computed with only one of the two structures. In fig. 5.5, effective masses are shown for the BB state together with fits of constants to the ground state plateaus and in fig. 5.6 for the Dd structure. We observe, that the ground state fits yield approximately the same ground state energy for same heavy quark separations and partly also the shape of the effective mass curves is similar. In general, larger (jackknife) errors occur for the Dd structure, especially for $r \gtrsim 7$ and thus, the plateau becomes more and more blurred. These findings are consistent with the assumed worse overlap of $\mathcal{O}_{Dd}$ with the tetraquark ground state for larger heavy quark separations.

In the past, effective masses for the BB structure with $\Gamma = (1 + \gamma_0)\gamma_5$ have already been computed within exactly the same lattice setup ("B40.24" ensemble), including the same choice for the smearing parameters [9]. Therefore it is a a good idea to compare my results to the previous ones. Double checking lattice QCD calculations always supports the credibility of results. The corresponding figures can be found in sec. A.5. Even for small euclidean

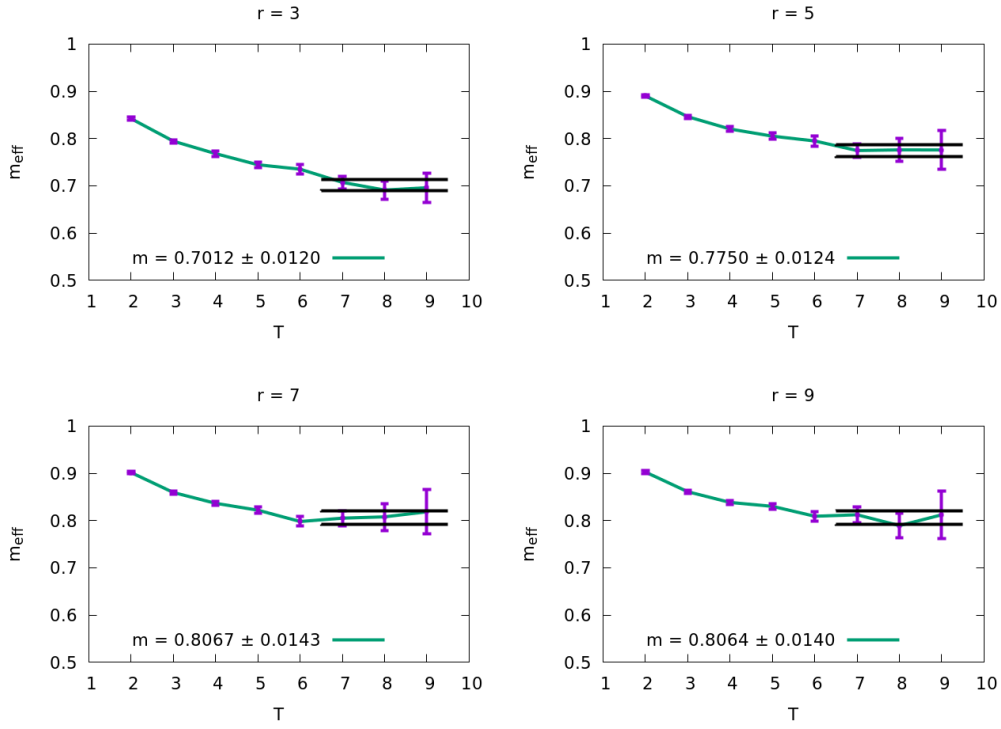

Figure 5.5: *Effective mass (in lattice units) together with ground state fits, resulting from an* 1×1 *correlation matrix for the BB operator with* $\Gamma_{BB} = (1+\gamma_0)\gamma_5$*. The results were produced using the "B40.24" ensemble.*

times, where the errors in the effective mass are very small, we find that the results are in accordance. For larger times, it is sufficient that the results agree within the error bars. Reconstructing the expectation values exactly is not possible due to the use of stochastic light quark propagators. The corresponding (randomly) generated stochastic sources are certainly not identical in both lattice computations.

Extracting the ground state for varying heavy quark separation leads to the potential of the static $\overline{b}\overline{b}$ pair in presence of the light quarks. The resulting potential is discussed in the following section.

5.5 Lattice potentials

As shown in the previous chapter, the potentials are extracted from effective mass plateaus at large eucliden times. Details of the shown potentials will of course depend on the quality of the fit. These circumstances will not be considered in the error bars, which are only jackknife errors, reflecting statistical uncertainties which arise because of solving the path integral over the gauge field using a finite number of gauge configurations.

From now on, all the ensembles, listed in tab. 4.1 are considered in the results. Moreover, data tables for the shown results can be found in the appendix, c.f. sec. A.6. Also the fit-ranges are collected in these tables. See sec. 4.2 for the choice of the smearing parameters.

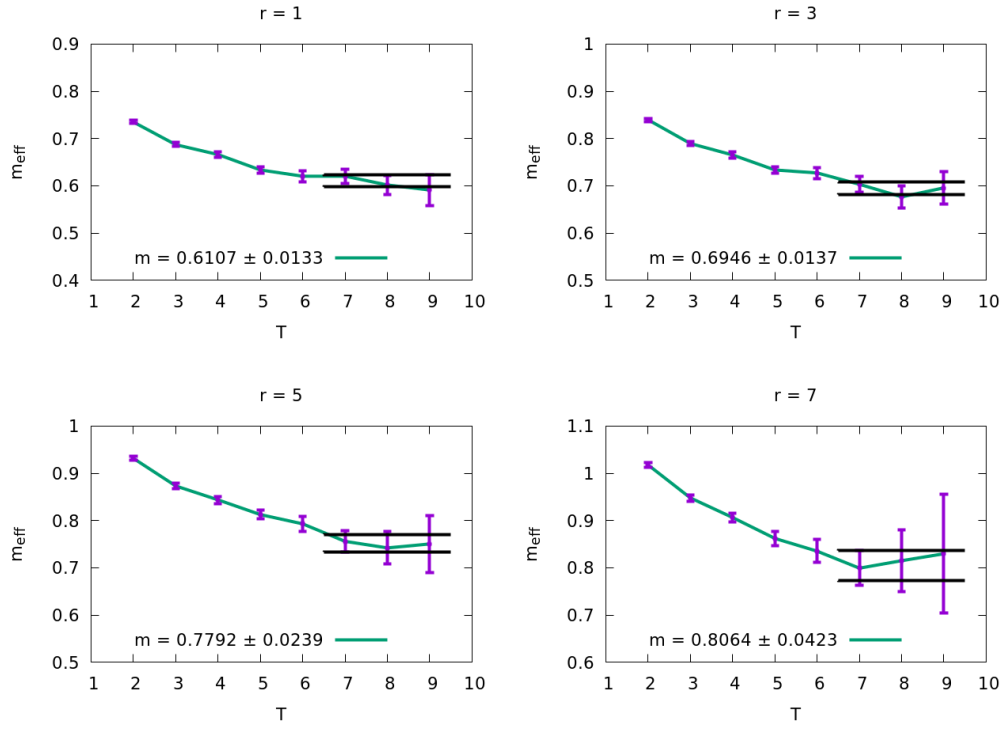

Figure 5.6: *Effective mass (in lattice units) together with ground state fits, resulting from an* 1×1 *correlation matrix for the Dd operator with* $\Gamma_{Dd} = (1 + \gamma_0)\gamma_5$*. The results were produced using the "B40.24" ensemble.*

We use the fact, that the BB potential yields twice the mass of the contributing mesons as threshold (here: $2m(S)$) to renormalise them. All potentials are shown with $2m(S)$ subtracted, i.e. in the BB potential, we find $V \to 0$ for large separations.

In fig. 5.7, an example plot for the potential is shown for the "D20.24" ensemble. We use this figure, to analyze and compare the potentials in detail. In general, we can expect that the potentials, evaluated with the mesonic molecule / diquark-antidiquark operators are (nearly) identical, because both structures describe the same quantum numbers. Indeed, we see that the potentials are in very good agreement (identical respecting the error bars) for small heavy quark separations. However, the potentials distinguish for larger separations, where the overlap of the Dd operator with the ground state starts getting worse. Here, we find a threshold in the BB potential, corresponding to twice the S meson mass, while for the Dd state an approximate linear increase of the potential occurs. This shape looks like a confining contribution, which arise due to the expansion of the static antidiquark (static colour charges). This is already a clear indication, that the Dd structure should be absent for large separations in the eigenvector-analysis.

In fig. 5.8, the potentials resulting from all three considered lattice ensembles are now shown together in one diagram. For small separations, the BB potentials as well as the Dd potentials are in very good agreement among themselves and allow us to combine the results in order

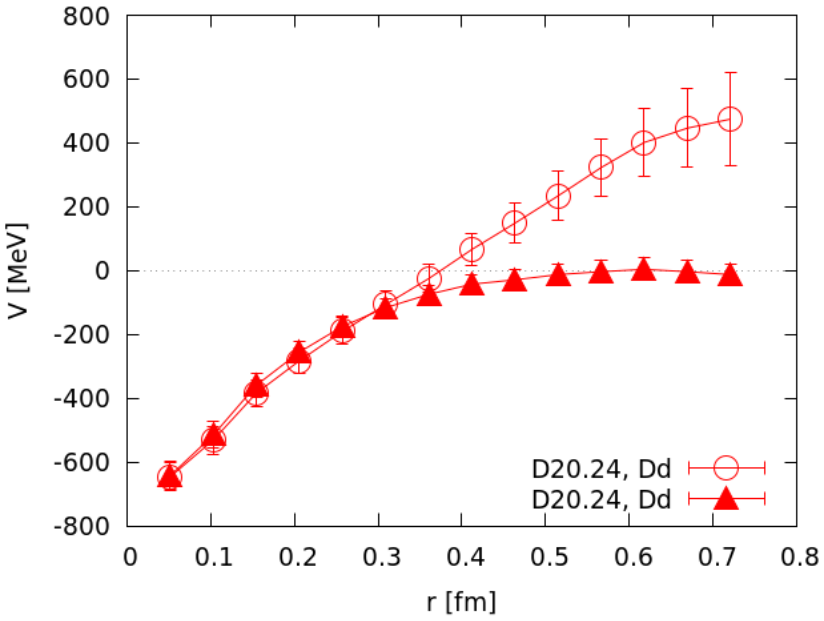

Figure 5.7: *Example plot for the effective potentials, resulting from the BB and Dd creation operators with $\Gamma_{BB} = (1+\gamma_0)\gamma_5$ and $\Gamma_{Dd} = (1+\gamma_0)\gamma_5$. The results are based on the "D20.24" ensemble.*

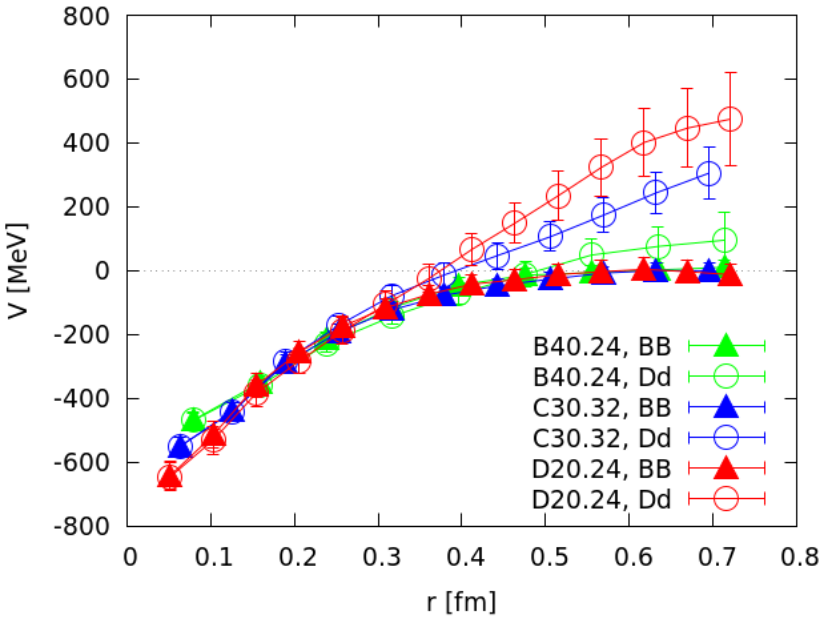

Figure 5.8: *Comparison of the BB / Dd potentials for all lattice ensembles, listed in tab. 4.1 and with $\Gamma_{BB} = (1+\gamma_0)\gamma_5$ and $\Gamma_{Dd} = (1+\gamma_0)\gamma_5$.*

to obtain a fine resolution of the potential. While the consistency remains for the mesonic molecule structure for larger separations, discrepancies in the diquark-antidiquark potentials occur. Here, we find an individual (approximate) linear increase for each of the lattice

ensembles. It is surprising, that the lattice with the largest spacing ("B40.24") leads to results very close to the ground state, while smaller lattice spacings lead to curves, far away from it. A possible explanation for this is that all smearing parameters kept fixed for all lattice simulations. That means, that the smaller the lattice spacing, the less smearing was effectively applied. We also have to keep in mind, that besides the lattice spacing, also the other parameters of the considered lattice ensembles were not exactly the same, e.g. the lattice sizes are different and pion masses are (slightly) different. This could also play a role in this context.

5.6 Eigenvector-analysis

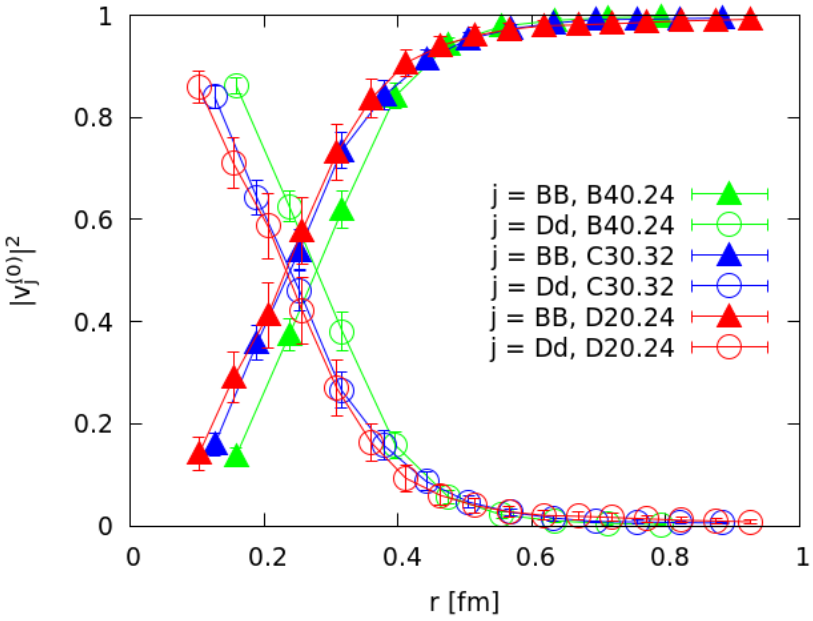

Figure 5.9: *Comparison of the BB structure with $\Gamma_{BB} = (1+\gamma_0)\gamma_5$ and the Dd structure with $\Gamma_{Dd} = (1+\gamma_0)\gamma_5$. The results are summarized for all ensembles, listed in tab. 4.1.*

Fig. 5.9 shows the entries of the ground state eigenvector or to be more precise the absolute square of its entries. These values were taken at large euclidean times, approximately the same time for all three lattice ensembles, see tab. A.10 for details. The almost excellent consistency of the results over the whole range of heavy quark separations, obtained using the different lattice ensembles is remarkable. This enables us to get a very fine resolution of the ground state eigenvector.

The $\bar{b}\bar{b}ud$ tetaquark state can be seen as a superposition of the mesonic molecule and the diquark-antidiquark structure, in which the eigenvector entries are the coefficients.

$$|\bar{b}\bar{b}ud; r\rangle \approx \sum_j v_0^j(t,t_0)\mathcal{O}_j^\dagger |0\rangle\,, \quad j \in \{BB, Dd\}$$

Therefore, we know that the absolute square of the entries of the normalized eigenvector can be used as weighting for the presence or absence for one of the tetraquark structures

compared to the other.

The shown results affirm our prediction that the diquark-antidiquark structure should be absent for large heavy quark separations (c.f. sec. 1.3 and sec. 5.4 - 5.5). Consequently, the tetraquark state is a pure mesonic molecule state in this limit. Analyzing the eigenvector for small separations is more instructive, because it is difficult to make predictions in this limit. Here, it turns out, that the Dd state is indeed the dominant contribution. We find $|v^{(0)}_{Dd}|^2 \approx 0.85$ for the smallest computed heavy quark separation. However, the Dd contribution rapidly gets smaller if the heavy quark separation is increased. At approximately $r \approx 0.25$ fm, both structures have equally represented and then the BB state starts to dominate the tetraquark state.

In the lattice simulations, which have led to this statements, the heavy quark separation was fixed by hand. In nature, the distance depends of course on the interactions in the four quark system. An interesting side note at this point is, that in previous studies of the static-light four quark system $\bar{b}\bar{b}ud$ system, the radial probability density to find the $\bar{b}\bar{b}$ antiquark pair at given separation has its peak at a value very close to the separation, where both states have the same weighting [7, 10].

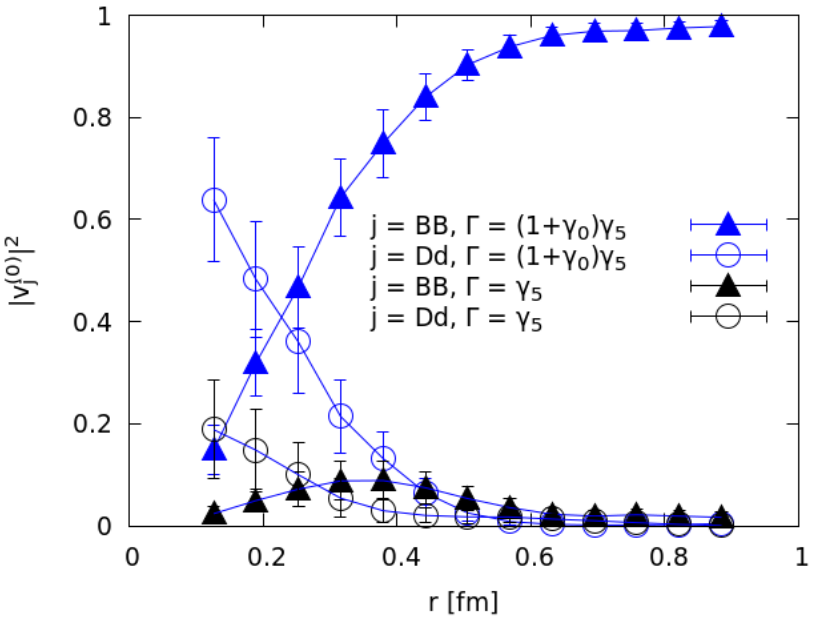

Figure 5.10: *Comparison of the BB structure with $\Gamma_{BB} \in \{(1+\gamma_0)\gamma_5,\ \gamma_5\}$ and the Dd structure with $\Gamma_{Dd} \in \{(1+\gamma_0)\gamma_5,\ \gamma_5\}$. The results are shown for the "C30.32" ensemble.*

Finally, we profit from having divided all computed correlation functions into several correlators, c.f. sec. 4.4. This enables us to recombine the correlators also to other Γ structures, here $\Gamma \in \{(1+\gamma_0)\gamma_5, \gamma_5\}$, without performing further lattice computations. In fig. 5.10, the results for the eigenvector-analysis of the corresponding 4×4 correlation matrix are presented. Shown are only results for the "C30.32" ensemble. Comparing the eigenvector for all three lattice ensembles in one diagram is not a good idea in this case, because we have four different curves in the diagram now, each with (large) error bars. Furthermore, we would not

profit from presenting results for different ensembles one after another, because they lead to the same qualitative findings, i.e. are consistent.

From fig. 5.10, we learn that the choice $\Gamma = (1 + \gamma_0)\gamma_5$ is much more significant in both tetraquark structures and $\Gamma = \gamma_5$ only leads to small contributions to the tetraquark state. For the BB system, one could already guess this result, because in previous studies of the BB potentials, it came out that $\Gamma = (1 + \gamma_0)\gamma_5$ leads to the most attractive potential with twice $2m(S)$ as threshold, which is also the most promising potential from the point of view of a bound tetraquark state [9]. However, for the Dd structure such a prediction was not possible. If one neglects the small contributions coming from $\Gamma = \gamma_5$, the analysis of the 2×2 / 4×4 matrices have led to the same qualitative statements, c.f. fig. 5.9 and fig. 5.10.

Since it turned out that $\Gamma = (1 + \gamma_0)\gamma_5$ corresponds to the dominant contributions for both structures, the previous more detailed analysis and comparison of these two creation operators throughout this whole section has gained in importance retrospectively, because this means, that we compared the most dominant contributions for both structure.

6 Conclusion

6.1 Summary

This work was aiming to expand previous lattice QCD studies concerning the static-light $\bar{b}\bar{b}ud$ four-quark system by investigating the internal structure of a predicted tetraquark bound state with quantum numbers $I(J^P) = 0(1^+)$. To this end, a diquark-antidiquark structure was compared to a mesonic molecule structure. The tetraquark (ground) state $|\bar{b}\bar{b}ud\rangle$ can be understood as linear combination of both structures, in which the coefficients are given by the (ground state-) eigenvector, resulting from the solution of the GEVP. The main result is, that the diquark-antidiquark structure dominates for small heavy quark separations, but it becomes more and more negligible for larger separations, so that the tetraquark can be seen as pure mesonic molecule state in this limit, c.f. sec. 5.6. Another interesting observation is, that both structures have approximately the same weight at the heavy quark separation, which is expected to be the most probable separation according to previous studies.

The absence of the diquark-antidiquark structure for large separations was not very surprising. Already in sec. 3, we could argue that the overlap of this structure with the ground state is expected to be small for large separations. Moreover, a worse signal-to-noise ratio, larger errors in the effective mass and discrepancies in the potentials affirmed this assumption before the eigenvector-analysis has started. However, the behavior for small separations was less predictable and hence the results in this limit are more instructive.

The performed numerical computations affirmed several predictions, e.g. the equality of both structures for vanishing heavy quark separation (c.f. sec. 5.3) and we successfully reproduced previous results from investigations of the BB systems (c.f. sec. A.5). Together with constantly checking symmetries of all computed correlators (c.f. sec. 5.1), the confirmations of expected phenomena and the reproduction of previous results support the credibility of the here performed lattice computations in a large amount.

6.2 Outlook

An obvious extension of this work would be the performance of the continuum limit and the extrapolation to physical quark masses. This was problematic in this work, because we used gauge field configurations, that differ both in their lattice spacing and light quark masses, c.f. tab. 4.1. Especially configurations with physical pion mass, which exist nowadays are interesting in this context. At least, we saw that the results are stable with respect to a variation of the lattice spacing. Furthermore, the pion mass for the "D20.24" was already comparably small (284 MeV).

The implementation of heavy quarks on the lattice could be improved, when the static approximation is dropped and Heavy Quark Effective Theory with $\mathcal{O}(1/m_h^2)$ corrections is considered. This would include corrections due to the heavy $\bar{b}\bar{b}$ spins, using lattice QCD. In Refs. [30, 31], this approach has been pioneered for the standard static quark-antiquark potential. However, this is expected to be a very challenging task for $\bar{b}\bar{b}qq$ four-quark systems.

In sec. 3.1, we saw that the presented operator for the diquark-antidiquark structure fails to represent arbitrary quantum numbers, since it vanishes for various Γ structures. Conse-

quently, modifications to the diquark-antidiquark creation operator would be necessary before more extensive studies of this structure could start.

Of course, studying the $B\bar{B}$ systems by means of lattice QCD would be desirable as a next step, because of the observation of such tetraquark candidates in experiments. However, due to the theoretical complexity of this systems and the lack of an promising strategy to handle them, it is more likely that theory and experiment get closer together if BB states are observed in present day laboratories in the near future.

A Appendix

A.1 Gamma matrices: Chiral representation

The euclidean gamma matrices obey the euclidean anti-commutation relations.

$$\{\gamma_\mu, \gamma_\nu\} = 2\delta_{\mu\nu}\mathbb{1}_4$$

We work explicitly in the chiral representation of the Dirac matrices, where γ_5 (the chirality operator) is diagonal.

$$\gamma_j = \begin{pmatrix} 0 & -i\sigma_j \\ +i\sigma_j & 0 \end{pmatrix} \quad , \quad \gamma_0 = \begin{pmatrix} 0 & -\mathbb{1}_2 \\ -\mathbb{1}_2 & 0 \end{pmatrix}$$

where σ_k are the Pauli matrices

$$\sigma_1 = \begin{pmatrix} 0 & +1 \\ +1 & 0 \end{pmatrix} \quad , \quad \sigma_2 = \begin{pmatrix} 0 & -i \\ +i & 0 \end{pmatrix} \quad , \quad \sigma_3 = \begin{pmatrix} +1 & 0 \\ 0 & -1 \end{pmatrix}$$

and

$$\gamma_5 = \gamma_0\gamma_1\gamma_2\gamma_3 = \begin{pmatrix} +\mathbb{1}_2 & 0 \\ 0 & -\mathbb{1}_2 \end{pmatrix}$$

In this representation, the gamma matrices obey ($\mu = 1, \ldots 5$)

$$\gamma_\mu = \gamma_\mu^\dagger = \gamma_\mu^{-1}$$

A.2 Closer view on the light flavour spin matrices

We investigate in what way the two spin matrices, combining the light quarks in the heavy-light correlation functions are related to each other. The results help to simplify the expressions for the correlation functions without affecting the general validity.

$$A \equiv C\Gamma$$
$$B \equiv \gamma_0\Gamma^\dagger C^\dagger\gamma_0 = \gamma_0 A^\dagger\gamma_0 = A^\dagger + \gamma_0[A^\dagger, \gamma_0] = A^\dagger + \{\Gamma^\dagger, \gamma_0\}\gamma_2$$

First of all, matrix A was used in the expression for matrix B. The representation $C = \gamma_0\gamma_2$ for the charge conjugation matrix was chosen, to further evaluate the expression.

$$\gamma_0[A^\dagger, \gamma_0] = \gamma_0\Gamma^\dagger\gamma_2\gamma_0\gamma_0 - \gamma_0\gamma_0\Gamma^\dagger\gamma_2\gamma_0 = \gamma_0\Gamma^\dagger\gamma_2 + \Gamma^\dagger\gamma_0\gamma_2 = \{\Gamma^\dagger, \gamma_0\}\gamma_2$$

Obviously, matrices A and B are the adjoint of each other, if $\Gamma^\dagger$ anti-commutes with γ_0.

$$\{\Gamma^\dagger, \gamma_0\} = 0 \quad \Longleftrightarrow \quad B = A^\dagger \quad \Longleftrightarrow \quad A = B^\dagger$$

Furthermore, if matrix A has definite properties under transposition, i.e. if it is symmetric or antisymmetric

$$A^T = (C\Gamma)^T = \pm C\Gamma = \pm A$$

matrix B adopts this property.

$$B^T = (\gamma_0 A^\dagger \gamma_0)^T = \gamma_0 (A^T)^\dagger \gamma_0 = \pm \gamma_0 A^\dagger \gamma_0 = \pm B$$

Since either both or neither of the matrices change their sign under transposition in this case, we can write

$$A_{\alpha\beta}\ B_{\gamma\delta} = (\pm A_{\beta\alpha}) \cdot (\pm B_{\delta\gamma}) = A_{\beta\alpha}\ B_{\delta\gamma} \tag{A.1}$$

This statement holds regardless of the choice for Γ, as long as A is either symmetric or antisymmetric. Consequently, this property allows to interchange the indices of both spin matrices A and B, without affecting the corresponding correlation function in any way. This equation also helps to identify the relations between correlators, that are connected via symmetries, c.f. sec. 4.4.

A.3 Mesonic molecule states

A.3.1 Meson content

Γ_X physical	meson content
γ_5	$-S_\uparrow S_\downarrow + S_\downarrow S_\uparrow - P_\uparrow P_\downarrow + P_\downarrow P_\uparrow$
$\gamma_0\gamma_5$	$-S_\uparrow S_\downarrow + S_\downarrow S_\uparrow + P_\uparrow P_\downarrow - P_\downarrow P_\uparrow$
1	$-S_\uparrow P_\downarrow + S_\downarrow P_\uparrow - P_\uparrow S_\downarrow + P_\downarrow S_\uparrow$
γ_0	$-S_\uparrow P_\downarrow + S_\downarrow P_\uparrow + P_\uparrow S_\downarrow - P_\downarrow S_\uparrow$
γ_3	$-iS_\uparrow S_\downarrow - iS_\downarrow S_\uparrow + iP_\uparrow P_\downarrow + iP_\downarrow P_\uparrow$
$\gamma_0\gamma_3$	$-iS_\uparrow S_\downarrow - iS_\downarrow S_\uparrow - iP_\uparrow P_\downarrow - iP_\downarrow P_\uparrow$
$\gamma_3\gamma_5$	$-iS_\uparrow P_\downarrow - iS_\downarrow P_\uparrow + iP_\uparrow S_\downarrow + iP_\downarrow S_\uparrow$
$\gamma_0\gamma_3\gamma_5$	$-iS_\uparrow P_\downarrow - iS_\downarrow P_\uparrow - iP_\uparrow S_\downarrow - iP_\downarrow S_\uparrow$
γ_1	$+iS_\uparrow S_\uparrow - iS_\downarrow S_\downarrow - iP_\uparrow P_\uparrow + iP_\downarrow P_\downarrow$
$\gamma_0\gamma_1$	$+iS_\uparrow S_\uparrow - iS_\downarrow S_\downarrow + iP_\uparrow P_\uparrow - iP_\downarrow P_\downarrow$
$\gamma_1\gamma_5$	$+iS_\uparrow P_\uparrow - iS_\downarrow P_\downarrow - iP_\uparrow S_\uparrow + iP_\downarrow S_\downarrow$
$\gamma_0\gamma_1\gamma_5$	$+iS_\uparrow P_\uparrow - iS_\downarrow P_\downarrow + iP_\uparrow S_\uparrow - iP_\downarrow S_\downarrow$
γ_2	$-S_\uparrow S_\uparrow - S_\downarrow S_\downarrow + P_\uparrow P_\uparrow + P_\downarrow P_\downarrow$
$\gamma_0\gamma_2$	$-S_\uparrow S_\uparrow - S_\downarrow S_\downarrow - P_\uparrow P_\uparrow - P_\downarrow P_\downarrow$
$\gamma_2\gamma_5$	$-S_\uparrow P_\uparrow - S_\downarrow P_\downarrow + P_\uparrow S_\uparrow + P_\downarrow S_\downarrow$
$\gamma_0\gamma_2\gamma_5$	$-S_\uparrow P_\uparrow - S_\downarrow P_\downarrow - P_\uparrow S_\uparrow - P_\downarrow S_\downarrow$

Table A.1: *Relation between the physical basis γ structure and the static-light meson content. For brevity, $P_{-;\downarrow/\uparrow}$ is denoted as $P_{\downarrow/\uparrow}$. (Table taken from [9].)*

A.3.2 Quantum numbers

		$\psi^{(f)}\psi^{(f')} = ud - du$		$\psi^{(f)}\psi^{(f')} \in \{uu\,,\, dd\,,\, ud + du\}$	
Γ	$\lvert j_z\rvert$	$\mathcal{P}$, $\mathcal{P}_x$	result	$\mathcal{P}$, $\mathcal{P}_x$	result
$\gamma_5 + \gamma_0\gamma_5$	0	$-$, $+$	A, SS	$+$, $+$	R, SS
1	0	$+$, $-$	A, SP	$-$, $-$	R, SP
$\gamma_3\gamma_5$	0	$+$, $+$	A, SP	$-$, $+$	R, SP
$\gamma_5 - \gamma_0\gamma_5$	0	$-$, $+$	A, PP	$+$, $+$	R, PP
$\gamma_3 + \gamma_0\gamma_3$	0	$+$, $-$	R, SS	$-$, $-$	A, SS
γ_0	0	$-$, $-$	R, SP	$+$, $-$	A, SP
$\gamma_0\gamma_3\gamma_5$	0	$-$, $+$	R, SP	$+$, $+$	A, SP
$\gamma_3 - \gamma_0\gamma_3$	0	$+$, $-$	R, PP	$-$, $-$	A, PP
$\gamma_1\gamma_5$	1	$+$, $-$	A, SP	$-$, $-$	R, SP
$\gamma_2\gamma_5$	1	$+$, $+$	A, SP	$-$, $+$	R, SP
$\gamma_2 + \gamma_0\gamma_2$	1	$+$, $-$	R, SS	$-$, $-$	A, SS
$\gamma_1 + \gamma_0\gamma_1$	1	$+$, $+$	R, SS	$-$, $+$	A, SS
$\gamma_0\gamma_1\gamma_5$	1	$-$, $-$	R, SP	$+$, $-$	A, SP
$\gamma_0\gamma_2\gamma_5$	1	$-$, $+$	R, SP	$+$, $+$	A, SP
$\gamma_2 - \gamma_0\gamma_2$	1	$+$, $-$	R, PP	$-$, $-$	A, PP
$\gamma_1 - \gamma_0\gamma_1$	1	$+$, $+$	R, PP	$-$, $+$	A, PP

Table A.2: *Quantum numbers of BB trial states; given are also combinations of Γ structures that lead to the cancellation of certain states; see also Tab. A.1. "result" characterizes the shapes of the numerically computed BB potentials (A: attractive potential; R: repulsive potential; SS: lower asymptotic value $2m(S)$; SP: higher asymptotic value $m(S) + m(P_-)$; PP: highest asymptotic value $2m(P_-)$). The states are ordered according to: (1) $|j_z| = 0, 1$, (2) attractive/repulsive potentials (for the flavour structure $ud - du$), (3) increasing asymptotic value of the potential, (4) $\mathcal{P}_x = -+$. (Table taken from [9].)*

$\Gamma_X^{(ud\pm du)}$ tb	$\mathcal{P}^{(\mathrm{tm})}$, $\mathcal{P}_x^{(\mathrm{tm})}$, sec.	$\Gamma_X^{(ud\pm du)}$ pb	$\mathcal{P}$, $\mathcal{P}_x$	type	mult.
$j_z = 0,\ I = 0$					
$\gamma_5^{(-)} - i\gamma_0^{(+)}$	$+,\ -,\quad a$	$(+\gamma_5 + \gamma_0\gamma_5)^{(-)}$	$-,\ +$	att SS	A
$\gamma_0\gamma_3\gamma_5^{(-)}$	$+,\ -,\quad a$	$+\gamma_0\gamma_3\gamma_5^{(-)}$	$-,\ +$	rep SP_-	A
$\gamma_5^{(-)} + i\gamma_0^{(+)}$	$+,\ -,\quad a$	$(+\gamma_5 - \gamma_0\gamma_5)^{(-)}$	$-,\ +$	att P_-P_-	A
$\gamma_0\gamma_3^{(-)} - i\gamma_3\gamma_5^{(+)}$	$-,\ +,\quad b$	$(+\gamma_0\gamma_3 + \gamma_3)^{(-)}$	$+,\ -$	rep SS	B
$1^{(-)}$	$-,\ +,\quad b$	$+1^{(-)}$	$+,\ -$	att SP_-	B
$\gamma_0\gamma_3^{(-)} + i\gamma_3\gamma_5^{(+)}$	$-,\ +,\quad b$	$(+\gamma_0\gamma_3 - \gamma_3)^{(-)}$	$+,\ -$	rep P_-P_-	B
$\gamma_3^{(+)}$	$-,\ -,\quad c$	$+i\gamma_3\gamma_5^{(-)}$	$+,\ +$	att SP_-	C
$\gamma_0\gamma_5^{(+)}$	$+,\ +,\quad d$	$+i\gamma_0^{(-)}$	$-,\ -$	rep SP_-	D
$j_z = 0,\ I = 1,\ I_z = 0$					
$\gamma_0\gamma_3^{(+)} - i\gamma_3\gamma_5^{(-)}$	$-,\ -,\quad c$	$(+\gamma_0\gamma_3 + \gamma_3)^{(+)}$	$-,\ -$	att SS	E
$1^{(+)}$	$-,\ -,\quad c$	$+1^{(+)}$	$-,\ -$	rep SP_-	E
$\gamma_0\gamma_3^{(+)} + i\gamma_3\gamma_5^{(-)}$	$-,\ -,\quad c$	$(+\gamma_0\gamma_3 - \gamma_3)^{(+)}$	$-,\ -$	att P_-P_-	E
$\gamma_5^{(+)} - i\gamma_0^{(-)}$	$+,\ +,\quad d$	$(+\gamma_5 + \gamma_0\gamma_5)^{(+)}$	$+,\ +$	rep SS	F
$\gamma_0\gamma_3\gamma_5^{(+)}$	$+,\ +,\quad d$	$+\gamma_0\gamma_3\gamma_5^{(+)}$	$+,\ +$	att SP_-	F
$\gamma_5^{(+)} + i\gamma_0^{(-)}$	$+,\ +,\quad d$	$(+\gamma_5 - \gamma_0\gamma_5)^{(+)}$	$+,\ +$	rep P_-P_-	F
$\gamma_0\gamma_5^{(-)}$	$+,\ -,\quad a$	$+i\gamma_0^{(+)}$	$+,\ -$	att SP_-	G
$\gamma_3^{(-)}$	$-,\ +,\quad b$	$+i\gamma_3\gamma_5^{(+)}$	$-,\ +$	rep SP_-	H
$j_z = 1,\ I = 0$					
$\gamma_0\gamma_{1/2}^{(-)} - i\gamma_{1/2}\gamma_5^{(+)}$	$-,\ -/+,\quad e/f$	$(+\gamma_0\gamma_{1/2} + \gamma_{1/2})^{(-)}$	$+,\ +/-$	rep SS	I
$\gamma_{2/1}^{(+)}$	$-,\ -/+,\quad e/f$	$+i\gamma_{2/1}\gamma_5^{(-)}$	$+,\ +/-$	att SP_-	I
$\gamma_0\gamma_{1/2}^{(-)} + i\gamma_{1/2}\gamma_5^{(+)}$	$-,\ -/+,\quad e/f$	$(+\gamma_0\gamma_{1/2} - \gamma_{1/2})^{(-)}$	$+,\ +/-$	rep P_-P_-	I
$\gamma_0\gamma_{1/2}\gamma_5^{(-)}$	$+,\ +/-,\quad g/h$	$\gamma_0\gamma_{1/2}\gamma_5^{(-)}$	$-,\ -/+$	rep SP_-	J
$j_z = 1,\ I = 1,\ I_z = 0$					
$\gamma_0\gamma_{1/2}^{(+)} - i\gamma_{1/2}\gamma_5^{(-)}$	$-,\ +/-,\quad f/e$	$(+\gamma_0\gamma_{1/2} + \gamma_{1/2})^{(+)}$	$-,\ +/-$	att SS	K
$\gamma_{2/1}^{(-)}$	$-,\ +/-,\quad f/e$	$+i\gamma_{2/1}\gamma_5^{(+)}$	$-,\ +/-$	rep SP_-	K
$\gamma_0\gamma_{1/2}^{(+)} + i\gamma_{1/2}\gamma_5^{(-)}$	$-,\ +/-,\quad f/e$	$(+\gamma_0\gamma_{1/2} - \gamma_{1/2})^{(+)}$	$-,\ +/-$	att P_-P_-	K
$\gamma_0\gamma_{1/2}\gamma_5^{(+)}$	$+,\ -/+,\quad h/g$	$\gamma_0\gamma_{1/2}\gamma_5^{(+)}$	$+,\ -/+$	att SP_-	L

Table A.3: *Twisted basis (tb) and physical basis (pb) quantum numbers for $ud\pm du$. Different physical basis multiplets are assigned capital letters, while different twisted mass sectors are assigned small letters. (Table taken from [9].)*

A.4 Symmetry checks of all computed correlators

$\hat{=}$	γ_5	$\mathcal{T}$	$\mathcal{P}$	$\mathcal{C}$
$C_1(+t)$	$+C_4^*(-t)$	$+C_4(-t)$	$+C_4(+t)$	$+C_1(-t)$
$C_2(+t)$	$+C_3^*(-t)$	$+C_3(-t)$	$+C_3(+t)$	$+C_2(-t)$
$C_3(+t)$	$+C_2^*(-t)$	$+C_2(-t)$	$+C_2(+t)$	$+C_3(-t)$
$C_4(+t)$	$+C_1^*(-t)$	$+C_1(-t)$	$+C_1(+t)$	$+C_4(-t)$
$C_5(+t)$	$+C_{12}^*(-t)$	$+C_8(-t)$	$-C_8(+t)$	$+C_9(-t)$
$C_6(+t)$	$-C_{11}^*(-t)$	$+C_7(-t)$	$-C_7(+t)$	$-C_{10}(-t)$
$C_7(+t)$	$-C_{10}^*(-t)$	$+C_6(-t)$	$-C_6(+t)$	$-C_{11}(-t)$
$C_8(+t)$	$+C_9^*(-t)$	$+C_5(-t)$	$-C_5(+t)$	$+C_{12}(-t)$
$C_9(+t)$	$+C_8^*(-t)$	$+C_{12}(-t)$	$-C_{12}(+t)$	$+C_5(-t)$
$C_{10}(+t)$	$-C_7^*(-t)$	$+C_{11}(-t)$	$-C_{11}(+t)$	$-C_6(-t)$
$C_{11}(+t)$	$-C_6^*(-t)$	$+C_{10}(-t)$	$-C_{10}(+t)$	$-C_7(-t)$
$C_{12}(+t)$	$+C_5^*(-t)$	$+C_9(-t)$	$-C_9(+t)$	$+C_8(-t)$
$C_{13}(+t)$	$+C_{16}^*(-t)$	$+C_{16}(-t)$	$+C_{16}(+t)$	$+C_{13}(-t)$
$C_{14}(+t)$	$+C_{15}^*(-t)$	$+C_{15}(-t)$	$+C_{15}(+t)$	$+C_{14}(-t)$
$C_{15}(+t)$	$+C_{14}^*(-t)$	$+C_{14}(-t)$	$+C_{14}(+t)$	$+C_{15}(-t)$
$C_{16}(+t)$	$+C_{13}^*(-t)$	$+C_{13}(-t)$	$+C_{13}(+t)$	$+C_{16}(-t)$

Table A.4: *Symmetry averaging for C_{11}, c.f. eq. 3.2.*

$\hat{=}$	γ_5	$\mathcal{T}$	$\mathcal{P}$	$\mathcal{C}$
$C_1(+t)$	$+C_4^*(-t)$	$+C_4(-t)$	$+C_4(+t)$	$+C_1(-t)$
$C_2(+t)$	$+C_2^*(-t)$	$+C_3(-t)$	$+C_3(+t)$	$+C_3(-t)$
$C_3(+t)$	$+C_3^*(-t)$	$+C_2(-t)$	$+C_2(+t)$	$+C_2(-t)$
$C_4(+t)$	$+C_1^*(-t)$	$+C_1(-t)$	$+C_1(+t)$	$+C_4(-t)$
$C_5(+t)$	$-C_{12}^*(-t)$	$-C_8(-t)$	$+C_8(+t)$	$+C_9(-t)$
$C_6(+t)$	$-C_{10}^*(-t)$	$-C_7(-t)$	$+C_7(+t)$	$+C_{11}(-t)$
$C_7(+t)$	$-C_{11}^*(-t)$	$-C_6(-t)$	$+C_6(+t)$	$+C_{10}(-t)$
$C_8(+t)$	$-C_9^*(-t)$	$-C_5(-t)$	$+C_5(+t)$	$+C_{12}(-t)$
$C_9(+t)$	$-C_8^*(-t)$	$-C_{12}(-t)$	$+C_{12}(+t)$	$+C_5(-t)$
$C_{10}(+t)$	$-C_6^*(-t)$	$-C_{11}(-t)$	$+C_{11}(+t)$	$+C_7(-t)$
$C_{11}(+t)$	$-C_7^*(-t)$	$-C_{10}(-t)$	$+C_{10}(+t)$	$+C_6(-t)$
$C_{12}(+t)$	$-C_5^*(-t)$	$-C_9(-t)$	$+C_9(+t)$	$+C_8(-t)$
$C_{13}(+t)$	$+C_{16}^*(-t)$	$+C_{16}(-t)$	$+C_{16}(+t)$	$+C_{13}(-t)$
$C_{14}(+t)$	$+C_{14}^*(-t)$	$+C_{15}(-t)$	$+C_{15}(+t)$	$+C_{15}(-t)$
$C_{15}(+t)$	$+C_{15}^*(-t)$	$+C_{14}(-t)$	$+C_{14}(+t)$	$+C_{14}(-t)$
$C_{16}(+t)$	$+C_{13}^*(-t)$	$+C_{13}(-t)$	$+C_{13}(+t)$	$+C_{16}(-t)$

Table A.5: *Symmetry averaging for C_{22}, c.f. eq. 3.4.*

$\hat{=}$	γ_5	$\mathcal{T}$	$\mathcal{P}$	$\mathcal{C}$
$C_1(+t)$	$+\mathbf{C_4^*}(-\mathbf{t})$	$+C_4(-t)$	$+C_4(+t)$	$+\mathbf{C_1}(-\mathbf{t})$
$C_2(+t)$	$+\mathbf{C_3^*}(-\mathbf{t})$	$+C_3(-t)$	$+C_3(+t)$	$+\mathbf{C_2}(-\mathbf{t})$
$C_3(+t)$	$+\mathbf{C_2^*}(-\mathbf{t})$	$+C_2(-t)$	$+C_2(+t)$	$+\mathbf{C_3}(-\mathbf{t})$
$C_4(+t)$	$+\mathbf{C_1^*}(-\mathbf{t})$	$+C_1(-t)$	$+C_1(+t)$	$+\mathbf{C_4}(-\mathbf{t})$
$C_5(+t)$	$-\mathbf{C_{12}^*}(-\mathbf{t})$	$-C_8(-t)$	$+C_8(+t)$	$+\mathbf{C_9}(-\mathbf{t})$
$C_6(+t)$	$-\mathbf{C_{11}^*}(-\mathbf{t})$	$-C_7(-t)$	$+C_7(+t)$	$+\mathbf{C_{10}}(-\mathbf{t})$
$C_7(+t)$	$-\mathbf{C_{10}^*}(-\mathbf{t})$	$-C_6(-t)$	$+C_6(+t)$	$+\mathbf{C_{11}}(-\mathbf{t})$
$C_8(+t)$	$-\mathbf{C_9^*}(-\mathbf{t})$	$-C_5(-t)$	$+C_5(+t)$	$+\mathbf{C_{12}}(-\mathbf{t})$
$C_9(+t)$	$+\mathbf{C_8^*}(-\mathbf{t})$	$+C_{12}(-t)$	$-C_{12}(+t)$	$+\mathbf{C_5}(-\mathbf{t})$
$C_{10}(+t)$	$+\mathbf{C_7^*}(-\mathbf{t})$	$+C_{11}(-t)$	$-C_{11}(+t)$	$+\mathbf{C_6}(-\mathbf{t})$
$C_{11}(+t)$	$+\mathbf{C_6^*}(-\mathbf{t})$	$+C_{10}(-t)$	$-C_{10}(+t)$	$+\mathbf{C_7}(-\mathbf{t})$
$C_{12}(+t)$	$+\mathbf{C_5^*}(-\mathbf{t})$	$+C_9(-t)$	$-C_9(+t)$	$+\mathbf{C_8}(-\mathbf{t})$
$C_{13}(+t)$	$-\mathbf{C_{16}^*}(-\mathbf{t})$	$-C_{16}(-t)$	$-C_{16}(+t)$	$+\mathbf{C_{13}}(-\mathbf{t})$
$C_{14}(+t)$	$-\mathbf{C_{15}^*}(-\mathbf{t})$	$-C_{15}(-t)$	$-C_{15}(+t)$	$+\mathbf{C_{14}}(-\mathbf{t})$
$C_{15}(+t)$	$-\mathbf{C_{14}^*}(-\mathbf{t})$	$-C_{14}(-t)$	$-C_{14}(+t)$	$+\mathbf{C_{15}}(-\mathbf{t})$
$C_{16}(+t)$	$-\mathbf{C_{13}^*}(-\mathbf{t})$	$-C_{13}(-t)$	$-C_{13}(+t)$	$+\mathbf{C_{16}}(-\mathbf{t})$

Table A.6: *Symmetry averaging for C_{12}, c.f. eq. 3.6. Correlators written in bold are related to correlators in C_{21}.*

$\hat{=}$	γ_5	$\mathcal{T}$	$\mathcal{P}$	$\mathcal{C}$
$C_1(+t)$	$+\mathbf{C_4^*}(-\mathbf{t})$	$+C_4(-t)$	$+C_4(+t)$	$+\mathbf{C_1}(-\mathbf{t})$
$C_2(+t)$	$+\mathbf{C_3^*}(-\mathbf{t})$	$+C_3(-t)$	$+C_3(+t)$	$+\mathbf{C_2}(-\mathbf{t})$
$C_3(+t)$	$+\mathbf{C_2^*}(-\mathbf{t})$	$+C_2(-t)$	$+C_2(+t)$	$+\mathbf{C_3}(-\mathbf{t})$
$C_4(+t)$	$+\mathbf{C_1^*}(-\mathbf{t})$	$+C_1(-t)$	$+C_1(+t)$	$+\mathbf{C_4}(-\mathbf{t})$
$C_5(+t)$	$+\mathbf{C_{12}^*}(-\mathbf{t})$	$+C_8(-t)$	$-C_8(+t)$	$+\mathbf{C_9}(-\mathbf{t})$
$C_6(+t)$	$+\mathbf{C_{11}^*}(-\mathbf{t})$	$+C_7(-t)$	$-C_7(+t)$	$+\mathbf{C_{10}}(-\mathbf{t})$
$C_7(+t)$	$+\mathbf{C_{10}^*}(-\mathbf{t})$	$+C_6(-t)$	$-C_7(+t)$	$+\mathbf{C_{11}}(-\mathbf{t})$
$C_8(+t)$	$+\mathbf{C_9^*}(-\mathbf{t})$	$+C_5(-t)$	$-C_5(+t)$	$+\mathbf{C_{12}}(-\mathbf{t})$
$C_9(+t)$	$-\mathbf{C_8^*}(-\mathbf{t})$	$-C_{12}(-t)$	$+C_{12}(+t)$	$+\mathbf{C_5}(-\mathbf{t})$
$C_{10}(+t)$	$-\mathbf{C_7^*}(-\mathbf{t})$	$-C_{11}(-t)$	$+C_{11}(+t)$	$+\mathbf{C_6}(-\mathbf{t})$
$C_{11}(+t)$	$-\mathbf{C_6^*}(-\mathbf{t})$	$-C_{10}(-t)$	$+C_{10}(+t)$	$+\mathbf{C_7}(-\mathbf{t})$
$C_{12}(+t)$	$-\mathbf{C_5^*}(-\mathbf{t})$	$-C_9(-t)$	$+C_9(+t)$	$+\mathbf{C_8}(-\mathbf{t})$
$C_{13}(+t)$	$-\mathbf{C_{16}^*}(-\mathbf{t})$	$-C_{16}(-t)$	$-C_{16}(+t)$	$+\mathbf{C_{13}}(-\mathbf{t})$
$C_{14}(+t)$	$-\mathbf{C_{15}^*}(-\mathbf{t})$	$-C_{15}(-t)$	$-C_{15}(+t)$	$+\mathbf{C_{14}}(-\mathbf{t})$
$C_{15}(+t)$	$-\mathbf{C_{14}^*}(-\mathbf{t})$	$-C_{14}(-t)$	$-C_{14}(+t)$	$+\mathbf{C_{15}}(-\mathbf{t})$
$C_{16}(+t)$	$-\mathbf{C_{13}^*}(-\mathbf{t})$	$-C_{13}(-t)$	$-C_{13}(+t)$	$+\mathbf{C_{16}}(-\mathbf{t})$

Table A.7: *Symmetry averaging for C_{21}, c.f. eq. 3.7. Correlators written in bold are related to correlators in C_{12}.*

A.5 Mesonic molecule: Comparison with previous results

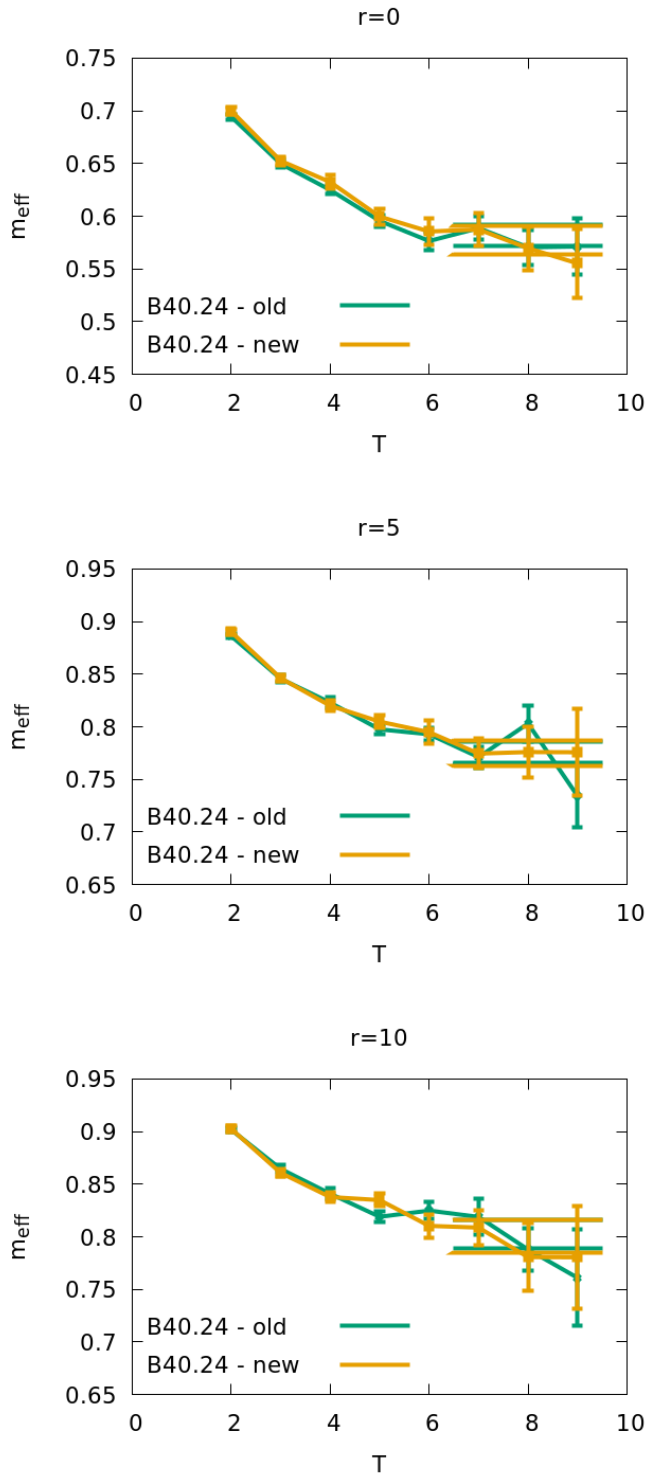

Figure A.1: *Comparison of computed effective masses with previous results within the same lattice setup ("B40.24"), including same smearing parameters.*

A.6 Data tables: Lattice potentials and eigenvector-analysis

	B40.24		C30.32		D20.24	
r	V_{BB} / 10^{-1}	σ / 10^{-3}	V_{BB} / 10^{-1}	σ/ 10^{-3}	V_{BB} / 10^{-1}	σ/ 10^{-3}
1	6.156	9.734	5.379	8.846	5.133	11.50
2	6.626	9.067	5.735	8.365	5.466	10.98
3	7.718	8.347	6.213	7.948	5.873	9.820
4	7.572	8.210	6.526	7.603	6.144	8.689
5	7.856	8.724	6.748	7.361	6.354	7.989
6	7.981	8.731	6.895	6.889	6.507	7.525
7	8.011	9.047	6.992	6.483	6.616	7.544
8	8.047	8.698	7.059	6.578	6.699	7.842
9	8.081	8.390	7.118	6.723	6.735	8.204
10			7.145	7.050	6.778	8.591
11			7.142	7.291	6.801	9.224
12					6.820	9.370

Table A.8: *Data tables for BB potentials in lattice units, resulting from 1×1 correlation matrices with $\Gamma_{BB} = (1+\gamma_0)\gamma_5$. The fit range for the ground state fits is $t \in [6, 9]$ in all cases.*

	B40.24		C30.32		D20.24	
r	V_{Dd} / 10^{-1}	σ / 10^{-3}	V_{Dd} / 10^{-1}	σ/ 10^{-3}	V_{Dd} / 10^{-1}	σ/ 10^{-3}
1	6.152	9.843	5.379	8.939	5.124	11.64
2	6.588	9.682	5.730	8.866	5.424	11.41
3	7.113	9.621	6.236	9.088	5.808	11.03
4	7.465	10.40	6.594	9.669	6.073	10.79
5	7.747	12.54	6.890	10.89	6.314	10.85
6	7.992	15.73	7.100	12.34	6.532	10.94
7	8.235	20.10	7.294	13.30	6.745	11.54
8	8.343	25.14	7.483	14.68	6.982	13.32
9	8.422	34.64	7.698	17.26	7.197	16.03
10			7.923	21.25	7.421	19.81
11			8.121	26.08	7.652	23.28
12					7.858	27.47

Table A.9: *Data tables for Dd potentials in lattice units, resulting from 1×1 correlation matrices with $\Gamma_{Dd} = (1+\gamma_0)\gamma_5$. The fit range for the ground state fits is $t \in [6, 9]$ in all cases.*

	B40.24		C30.32		D20.24	
r	$v_0^{(BB)}/10^{-1}$	$\sigma/10^{-2}$	$v_0^{(BB)}/10^{-1}$	$\sigma/10^{-2}$	$v_0^{(BB)}/10^{-1}$	$\sigma/10^{-2}$
2	1.380	1.599	1.598	2.232	1.413	3.174
3	3.743	3.077	3.575	3.384	2.898	4.937
4	6.194	3.752	5.390	4.001	4.131	6.394
5	8.423	2.507	7.347	3.523	5.788	6.508
6	9.437	1.275	8.425	2.838	7.306	5.490
7	9.785	0.645	9.129	1.859	8.370	3.749
8	9.901	0.411	9.533	1.143	9.066	2.643
9	9.950	0.266	9.734	0.725	9.400	1.927
10	9.974	0.165	9.844	0.507	9.602	1.497
11			9.916	0.203	9.722	1.146
12			9.920	0.292	9.794	0.894
13			9.935	0.240	9.811	0.782
14			9.944	0.234	9.834	0.733
15					9.862	0.644
16					9.889	0.540
17					9.094	0.480
18					9.920	0.452

Table A.10: *Absolute square of the ground state eigenvector entries, resulting from a* 2×2 *correlation matrix with* $\Gamma_{BB} = (1+\gamma_0)\gamma_5$ *and* $\Gamma_{Dd} = (1+\gamma_0)\gamma_5$*. Only the* BB *entry is shown and the* Dd *entry is simply* $|v_0^{Dd}|^2 = 1 - |v_0^{BB}|^2$ *with the same uncertainty. The values were taken at* $t = 7$ */* $t = 8$ */* $t = 9$ *for the "B40.24" / "C30.32" / "D20.24" ensembles.*

	BB, $\Gamma = (1+\gamma_0)\gamma_5$		BB, $\Gamma = \gamma_5$		Dd, $\Gamma = (1+\gamma_0)\gamma_5$		Dd, $\Gamma = \gamma_5$	
r	$v_0/10^{-1}$	$\sigma/10^{-2}$	$v_0/10^{-1}$	$\sigma/10^{-2}$	$v_0/10^{-1}$	$\sigma/10^{-2}$	$v_0/10^{-1}$	$\sigma/10^{-2}$
2	1.492	4.846	0.240	1.464	6.382	12.13	1.885	9.605
3	3.193	6.480	0.497	2.301	4.827	11.28	1.483	8.903
4	4.674	7.960	0.721	3.309	3.603	10.18	1.003	6.325
5	6.431	7.594	0.882	3.756	2.143	7.164	0.544	3.764
6	7.489	6.734	0.890	3.755	1.323	5.103	0.299	2.293
7	8.397	4.677	0.749	3.162	6.482	2.884	0.206	1.510
8	9.030	3.020	0.537	2.398	2.558	1.150	0.177	1.244
9	9.383	2.229	0.358	1.845	0.842	0.736	0.174	1.142
10	9.607	1.720	0.284	1.363	0.308	0.410	0.134	0.920
11	9.689	1.478	0.193	1.199	0.164	0.260	0.101	0.680
12	9.700	1.418	0.218	1.234	0.181	0.239	0.064	0.524
13	9.751	1.257	0.193	1.152	0.262	0.270	0.030	0.343
14	9.780	1.249	0.168	1.150	0.451	0.368	0.007	0.167

Table A.11: *Absolute square of the ground state eigenvector entries, resulting from a* 4×4 *correlation matrix. The values were taken at* $t = 8$ *for the "C30.32" ensemble.*

References

[1] J. Beringer et al. [Particle Data Group], Phys. Rev. D **86**, 010001 (2012)

[2] K. A. Olive et al. [Particle Data Group], Chin. Phys. C **38**, 090001 (2014)

[3] A. Bondar et al. [Belle Collaboration], Phys. Rev. Lett. **108**, 122001 (2012), arXiv:1110.2251 [hep-ex]

[4] Z. Q. Liu et al. [Belle Collaboration], Phys. Rev. Lett. **110**, 252002 (2013), arXiv:1304.0121 [hep-ex]

[5] K. Chilkin et al. [Belle Collaboration], Phys. Rev. D **90**, 112009 (2014), arXiv:1408.6457 [hep-ex]

[6] D. V. Bugg, Europhys. Lett. **96**, 11002 (2011), arXiv:1105.5492 [hep-ph]

[7] P. Bicudo, M. Wagner, Phys. Rev. D **87**, 114511 (2013), arXiv:1209.6274 [hep-ph]

[8] P. Bicudo, K. Cichy, A. Peters, B. Wagenbach, M. Wagner, Phys. Rev. D **92**, 014507 (2015), arXiv:1505.00613 [hep-lat]

[9] P. Bicudo, K. Cichy, A. Peters, M. Wagner, Phys. Rev. D **93**, 034501 (2016), arXiv:1510.03441 [hep-lat]

[10] P. Bicudo, J. Scheunert, M. Wagner, Phys. Rev. D **95**, 034502 (2017), arXiv:1612.02758 [hep-lat]

[11] Z. S. Brown, K. Orginos, Phys. Rev. D **86**, 114506 (2012), arXiv:1210.1953 [hep-lat]

[12] A. Francis, R. J. Hudspith, R. Lewis, K. Maltman, (2016), arXiv:1607.05214[hep-lat]

[13] P. Weisz, Nucl. Phys. B **212**, 1 (1983)

[14] A. Shindler, Phys. Rept. **461**, 37 (2008), arXiv:0707.4093 [hep-lat]

[15] R. Frezzotti, P. A. Grassi, S. Sint, P. Weisz, JHEP **0108**, 058 (2001), arXiv:hep-lat/0101001

[16] R. Frezzotti, G. C. Rossi, JHEP **0408**, 007 (2004), arXiv: 0707.4093 [hep-lat]

[17] E. Eichten, B. Hill, Phys. Lett. B **234**, 511 (1990)

[18] M. Della Morte, A. Shindler, R. Sommer, JHEP **0508**, 051 (2005), arXiv:hep-lat/0506008

[19] M. Della Morte, S. Dürr, J. Heitger, H. Molke, J. Rolf, A. Shindler, R. Sommer, Phys. Lett B **581** (2004) 93, hep-lat/0307021

[20] B. Blossier, M. Della Morte, G. von Hippel, T. Mendes and R. Sommer, JHEP **0904**, 094 (2009), arXiv: hep-lat/0306014

[21] V. M. Abazov et al. [D0 Collaboration], Phys. Rev. Lett. **99**, 172001 (2007), arXiv:0705.3229 [hep-ex]

[22] T. Aaltonen et al. [CDF Collaboration], Phys. Rev. Lett. **100**, 082001 (2008), arXiv:0710.4199 [hep-ex]

[23] Ph. Boucaud et al. [ETM Collaboration], Phys. Lett. B **650**, 304 (2007), arXiv:hep-lat/0701012

[24] M. Albanese et al. [APE Collaboration], Phys. Lett. B **192**, 163 (1987)

[25] S. Gusken, Nucl. Phys. Proc. Suppl. **17** 361 (1990)

[26] C. Alexandrou et al. [ETM Collaboration], Phys. Rev. D **78**, 014509 (2008), arXiv:0803.3190

[27] A. Hasenfratz, F. Knechtli, Phys. Rev. D **64**, 034504, (2001), arXiv:hep-lat/0103029

[28] A. Hasenfratz, F. Knechtli, Comput. Phys. Commun. **148** 81-86 (2002), arXiv:hep-lat/0203010

[29] A. Abdel-Rehim, C. Alexandrou, J. Berlin, M. Dalla Brida, J. Finkenrath, M. Wagner, Comput. Phys. Commun. **220**, 97 (2017), arXiv:1701.07228 [hep-lat]

[30] Y. Koma, M. Koma, H. Wittig, Phys. Rev. Lett. **97**, 122003 (2006), arXiv:hep-lat/0607009

[31] Y. Koma, M. Koma, Nucl. Phys. B **769**, 79 (2007), arXiv:hep-lat/0609078

[32] A. Ali, J.S. Lange, S. Stone, Prog. Part. Nucl. Phys. **97**, 123 (2017), arXiv:1706.00610 [hep-ph]

[33] C. Gattringer, C. B. Lang, "Quantum Chromodynamics on the Lattice", Lect. Notes Phys. **788**, 1 (2010)

[34] H. J. Rothe, "Lattice gauge theories: An Introduction", World Sci. Lect. Notes Phys. **43**, 1 (1992)

[35] https://itp.uni-frankfurt.de/∼mwagner/talks/Trento_2017.pdf

[36] https://itp.uni-frankfurt.de/∼mwagner/research.html

Danksagung

An dieser Stelle möchte ich mich herzlich bei Prof. Marc Wagner für die ausgezeichnete Betreuung meiner Arbeit bedanken. In jeder der zahlreichen und teils längeren Diskussionen blieb schließlich keine meiner Fragen unbeantwortet. Ich bin ebenfalls für die vielen Ratschläge dankbar, die zur Gestaltung der Arbeit beigetragen haben.

Auch bei Prof. Owe Philipsen, der freundlicherweise die Zweitkorrektur dieser Arbeit übernimmt, möchte ich mich hierfür bedanken.

Desweiteren danke ich Martin Pflaumer für hilfreiche Gespräche vor allem zu Beginn meiner Arbeit. Das hat es mir ermöglicht, schnell den Umgang mit dem GOETHE-HLR Computercluster zu erlernen und die für mich notwendigen Programme zu konfigurieren. Ebenfalls bin ich Dr. Antje Peters sehr dankbar für das zeitintensive Durchstöbern meiner Unterlagen, wann immer ich Detailfragen hierzu hatte.

Meinen Kommilitonen und Freunden Gabriel Porebski, Yannick Dengler und Alena Zmarsly, die mich bereits seit Beginn des Studiums begleiten, spreche ich für unzählige aufschlussreiche Unterhaltungen, neue Denkanstöße und eine schöne Zeit meinen Dank aus.

Selbstverständlich bin ich auch meiner Familie, insbesondere meinen Eltern für die Unterstützung während des gesamten Studiums, den mentalen Rückhalt und für das Korrekturlesen meiner Arbeiten sehr dankbar.

Selbstständigkeitserklärung

Hiermit versichere ich, die vorliegende Arbeit gemäß §30(12) der Ordnung für den Bachelor- und den Masterstudiengang Physik der Johann Wolfgang Goethe-Universität Frankfurt am Main vom 24.04.2013 selbständig und ohne Benutzung anderer als der angegebenen Quellen und Hilfsmittel verfasst zu haben. Alle Stellen, Bilder und Zeichnungen, die wörtlich oder sinngemäß aus Veröffentlichungen oder aus anderen fremden Texten entnommen wurden, wurden als solche kenntlich gemacht. Diese Abschlussarbeit ist nicht, auch nicht auszugsweise, für eine andere Prüfung oder Studienleistung verwendet worden.

Datum	Unterschrift